OPTIMIZATION OF AIR INTAKE SYSTEM FOR INLINE-4 DIESEL ENGINE

WAN MUHAMAD IRFAN HILMI BIN WAN HARUN

Thesis submitted in partial fulfillment of the requirements
for the award of the degree of
Bachelor of Mechanical Engineering with Automotive Engineering

Faculty of Mechanical Engineering

UNIVERSITI MALAYSIA PAHANG

JUNE 2012

UNIVERSITI MALAYSIA PAHANG

FACULTY OF MECHANICAL ENGINEERING

We certify that the project entitled “Optimization of Air Intake System for Inline-4 Diesel Engine” is written by Wan Muhamad Irfan Hilmi Bin Wan Harun. We have examined the final copy of this project and in our opinion; it is fully adequate in terms of scope and quality for the award of the degree of Bachelor of Engineering. We herewith recommend that it be accepted in partial fulfillment of the requirements for the degree of Bachelor of Mechanical Engineering with Automotive Engineering.

Mr. AMIR ABDUL RAZAK

Examiner Signature

SUPERVISOR'S DECLARATION

"I hereby declare that I have read this thesis and in my opinion this thesis sufficient in terms of scope and quality for the award the degree of Bachelor of Mechanical Engineering with Automotive Engineering"

Signature : ……

Name of Supervisor : Dr. RIZALMAN BIN MAMAT

Position : LECTURER

Date : 14 JUNE 2012

STUDENT'S DECLARATION

I declare that this thesis entitled Optimization of Air Intake System for Inline-4 Diesel Engine is the result of my own research except as cited in the references. The thesis has not been accepted for any degree and is not concurrently submitted in candidature of any other degree.

Signature : …….

Name of Candidate : WAN MUHAMAD IRFAN HILMI BIN WARUN

ID Number : MH08076

Date : 14 JUNE 2012

Dedicated to my parents

Mr. Wan Harun bin Wan Yaacob

Mrs. Haminih@Mariati binti Warimin

ACKNOWLEDGEMENT

I would like to express my deepest appreciation and gratitude to my supervisor, Dr. Rizalman Bin Mamat for his guidance, patience for giving advises and supports throughout the progress of this project. Special thanks are also given to all lecturers and vocational trainers for the guidance, experience sharing and comment on my project thesis. They were not hesitant to answer all my doubts and spending their time to guide me during my experimental work.

A great appreciation is acknowledged to the Faculty of Mechanical Engineering for the funding under the final year project.

Last but not least, I would like to thank all my friends and my family for their support and encouragement given to me, especially during the hard times.

ABSTRACT

Air Intake System is a system that produces fresh and clean air to an engine for combustion process. Insufficient air into the combustion chamber will decrease the engine performance thus decrease power generated by the engine. For this thesis, the objective is to study the effect of pressure drop inside the air intake system. Simulation and experiment methods have been conducted in this study. Air intake system model that had been use in this study is the air intake system of Proton Waja and this study focus on optimization of the air box. Data that have been obtained from simulation analysis was used to fabricate an optimized design of an air box. This air box then will be tested on an experiment test. All the data from simulation and experiment testing were collected and analyze. From the analysis, by adding guide vane and bell mouth on a standard air box, the pressure drop can be decreased thus increase the air flow performance inside the air intake system. In further study, it was recommended to test the optimized air box on Proton Waja to see the actual performance increased.

ABSTRAK

Sistem Induksi Udara adalah satu sistem yang berperanan untuk membekalkan udara yang bersih dengan kuantiti yang mencukupi untuk dibakar di dalam kebuk pembakaran enjin. Kadar penyaluran udara yang kurang ke dalam enjin akan mengurangkan kadar keberkesanan pembakaran bahan bakar di dalam enjin seterusnya menyebabkan enjin tidak dapat menghasilkan kuasa yang maksimum. Tesis ini bertujuan untuk mengkaji kesan perbezaan tekanan di dalam sistem induksi udara. Kaedah yang telah digunakan di dalam kajian ini adalah kaedah simulasi dan eksperimen. Model sistem induksi udara yang digunakan di dalam kajian ini diambil daripada model kenderaan Proton Waja dan kajian ini mengfokuskan kepada kotak penapisan udara. Maklumat-maklumat yang diperoleh daripada analisis simulasi digunakan untuk membina sebuah kotak udara yang lebih baik dan diuji di dalam eksperimen. Maklumat- maklumat yang diperoleh daripada kajian simulasi dan eksperimen kemudiannya dikumpul dan dianalisa. Daripada analisa yang telah dijalankan, dengan pemasangan mulut loceng dan sirip pandu keatas sistem induksi udara yang asal dapat mengurangkan perbezaan tekanan di dalam sistem induksi udara. Kajian yang lebih terperinci disarankan bagi melihat keberkesanan sistem induksi udara yang telah dioptimumkan ini dengan ujian prestasi ke atas kereta Proton Waja.

TABLE OF CONTENTS

	Page
TITLE	**i**
EXAMINER'S DECLARATION	**ii**
SUPERVISOR'S DECLARATION	**iii**
STUDENT'S DECLARATION	**iv**
DEDICATION	**v**
ACKNOWLEDGEMENTS	**vi**
ABSTRACT	**vii**
ABSTRAK	**viii**
TABLE OF CONTENTS	**ix**
LIST OF TABLES	**xiii**
LIST OF FIGURES	**xiv**
LIST OF SYMBOLS	**xviii**
LIST OF ABBREVIATIONS	**xix**

CHAPTER 1 INTRODUCTION

1.1	Introduction	1
1.2	Problem statement	2
1.3	Objectives	3
1.4	Scopes	3
1.5	Hypothesis	3
1.6	Methodology	4

CHAPTER 2 LITERATURE REVIEW

2.1 Introduction 5

2.2 Air Intake System 5

2.2.1 Theory of Pulsating Flow 12

2.2.2 Steady Flow Test 13

2.3 Bernoulli Equation 14

2.3.1 Major Loss 15

2.3.2 Minor Loss 16

2.3.3 Total Pressure 17

2.4 Mass and Volume Flow Rate 18

2.5 Computational Fluid Dynamics (CFD) 19

2.5.1 Governing Equations 22

2.5.2 Conservation of Mass 22

2.5.3 Conservation of Momentum 23

2.5.4 Energy equation 24

2.5.5 Two-Equation Model: k-ε Model 25

2.5.6 Model of Turbulence 26

2.5.7 Near-Wall Treatment 29

2.5.8 Simulation Benefits 31

CHAPTER 3 METHODOLOGY

3.0 General Methodology 32

3.1 Literature Study 33

3.2 Flow Chart 34

3.3 Data Collecting 35

3.4 3D Design Modelling 36

3.5 CFD Simulation Setup 39

3.5.1 Design Modeller 39

3.5.2 Computational Mesh Generation Setting 41

3.5.3 Meshes Refinement 42

3.5.4 Boundary Condition Setting Simulation 43

3.5.5 Air Flow Simulation 47

3.6 Model Fabrication 48

3.6.1 Guide vane 48

3.6.2 Bell mouth 50

3.7 Experimental Setup 52

CHAPTER 4 RESULTS AND DISCUSSIONS

4.1 Introduction 56

4.2 Calculation of Air Velocity 56

4.3 Results 59

4.3.1 CFD Simulation result 59
4.3.2 Experimental results 71
4.4 Discussions 78
4.4.1 CFD analysis 78
4.4.2 Flow bench test analysis 79

CHAPTER 5 CONCLUSION AND RECOMMENDATIONS

5.1 Conclusions 80
5.2 Recommendations 81

REFERENCES

APPENDICES

A GANTT CHART FOR FINAL YEAR PROJECT (FYP) 1
B GANTT CHART FOR FINAL YEAR PROJECT (FYP) 2

LIST OF TABLES

Table No.	Title	Page
3.1	Specifications of flow bench system	54
4.1	Table of volume flow rate (m^3/s), mass flow rate (kg/s), and outlet velocity (m/s) for 1000 RPM until 7000 RPM.	58
4.2	Result of pressure drop for CFD analysis on standard air box at 1000 RPM until 7000 RPM	59
4.3	Result of pressure drop for CFD analysis on optimized air box (Guide vane and bell mouth) at 1000 RPM until 7000 RPM	59
4.4	Result of pressure drop for CFD analysis on optimized air box (Guide vane only) at 1000 RPM until 7000 RPM	60
4.5	Result of pressure drop for CFD analysis on optimized air box (Bell moth only) at 1000 RPM until 7000 RPM	60
4.6	Result of pressure drop for flow bench test on standard air box at valve lift 0.001 m until 0.008 m	71
4.7	Result of pressure drop for flow bench test on optimized air box with guide vane and bell mouth at valve lift 0.001 m until 0.008 m	71
4.8	Result of pressure drop for flow bench test on optimized air box with guide vaneat valve lift 0.001 m until 0.008 m	72
4.9	Result of pressure drop for flow bench test on optimized air box with bell mouth at valve lift 0.001 m until 0.008 m	72

LIST OF FIGURES

Figure No.	Title	Page
2.1	Rib pattern inside air box	6
2.2	3D geometry of air intake system	7
2.3	Guide vane placement by previous study	8
2.4	Pressure drop vs Airflow for a Typical Dry Air Filter in fresh condition	9
2.5	Velocity vector plot:	
	(a) with baffle (guide vane) installation	9
	(b) without baffle (guide vane) installation	10
2.6	Velocity vector plot:	
	(a) near outlet without bell mouth;	11
	(b) near outlet after introducing bell mouth	11
2.7	Pressure drop, single-mitered steel elbows, and curved rubber elbows at 1000 cfm	12
2.8	Steady flow test bench diagram	14
2.9	Velocity profile as function of distance normal to the wall in the turbulent boundary layer	30
3.1	Flow Chart	34
3.2	Proton Waja Air Box	35
3.3	3D Design of air box	36
3.4	Air box lower part	37
3.5	Filter bed	37
3.6	Upper part of air box	38

3.7	(a) Upper part air box with bell mouth, (b) Lower part air box with guide vane	38 38
3.8	Air box in CFD model	40
3.9	Air box in CFD design modeller	40
3.10	Air box in CFD meshing	41
3.11	Air box mesh structure	42
3.12	Detail of mesh sizing in AnSYS Fluent	43
3.13	Detail of mesh inflation in AnSYS Fluent	43
3.14	Boundary condition setting on pressure inlet for inlet zone	46
3.15	Boundary condition setting on velocity inlet for outlet zone	46
3.16	Solution method for Air box simulation	47
3.17	Solution initialization for Air box simulation	48
3.18	Guide vane design in SolidWork.	49
3.19	Fabricated guide vane	49
3.20	Guide vane installation on lower part of air box	50
3.21	Bell mouth design on SolidWork	51
3.22	Fabricated bell mouth	51
3.23	Fabricated bell mouth installation on upper part air box	52
3.24	Cylinder head setting on head adapter on flow bench test	53
3.25	Air box setting on flow bench test	53
3.26	Air box setting on flow bench test diagram	54
3.27	Multitube Manometer model SOLTEQ FM21-VT-A	55
3.28	Dial gauge on valve lift controller; model OXFORD 300-852	55
4.1	Graph of pressure drop versus RPM for CFD analysis on standard air box and optimized air box with guide vane and bell mouth at 1000 RPM until 7000 RPM	61
4.2	Graph of pressure drop versus RPM for CFD analysis on standard air box and optimized air box with bell mouth at 1000 RPM until 7000 RPM	61

4.3	Graph of pressure drop versus RPM for CFD analysis on standard air box and optimized air box with guide vane at 1000 RPM until 7000 RPM	62
4.4	Graph of pressure drop versus RPM for CFD analysis on optimized air box with bell mouth and optimized air box with guide vane at 1000 RPM until 7000 RPM	62
4.5	Graph of pressure drop versus RPM for CFD analysis on optimized air box with bell mouth and optimized air box with bell mouth and guide vane at 1000 RPM until 7000 RPM	63
4.6	Graph of pressure drop versus RPM for CFD analysis on optimized air box with guide vane and optimized air box with bell mouth and guide vane at 1000 RPM until 7000 RPM	63
4.7	Graph of pressure drop versus RPM for CFD analysis on standard air box, optimized air box with bell mouth, optimized air box with guide vane, and optimized air box with bell mouth and guide vane at 1000 RPM until 7000 RPM	64
4.8	Velocity magnitude (m^2/s) contour plot: (a) lower part optimize air box with bell mouth and guide vane; (b) upper part optimize air box with bell mouth and guide vane	65
4.9	Velocity magnitude (m^2/s) contour plot: (a) lower part optimize air box with guide vane; (b) upper part optimize air box with guide vane	66
4.10	Velocity magnitude (m^2/s) contour plot: (a) lower part optimize air box with bell mouth; (b) upper part optimize air box with bell mouth	67
4.11	Velocity magnitude (m^2/s) contour plot: (a) lower part standard air box; (b) upper part standard air box	68
4.12	Velocity magnitude (m^2/s) vector plot: (a) lower part air box without guide vane; (b) lower part air box with guide vane	69
4.13	Velocity magnitude (m^2/s) vector plot: (a) upper part air box without bell mouth; (b) upper part air box with bell mouth	70
4.14	Graph of pressure drop versus valve lift for flow bench test on standard air box and optimized air box with guide vane and bell mouth at 0.001 m valve lift until 0.008 m valve lift.	73

4.15	Graph of pressure drop versus valve lift for flow bench test on standard air box and optimized air box with guide vane at 0.001 m valve lift until 0.008 m valve lift.	73
4.16	Graph of pressure drop versus valve lift for flow bench test on standard air box and optimized air box with bell mouth at 0.001 m valve lift until 0.008 m valve lift.	74
4.17	Graph of pressure drop versus valve lift for flow bench test on optimized air box with guide vane and bell mouth and optimized air box with guide vane at 0.001 m valve lift until 0.008 m valve lift.	74
4.18	Graph of pressure drop versus valve lift for flow bench test on optimized air box with guide vane and bell mouth and optimized air box with bell mouth at 0.00 1m valve lift until 0.008 m valve lift.	75
4.19	Graph of pressure drop versus valve lift for flow bench test on optimized air box with guide vane and optimized air box with bell mouth at 0.001 m valve lift until 0.008 m valve lift.	75
4.20	Graph of pressure drop versus valve lift for flow bench test on standard air box, optimized air box with guide vane and bell mouth, optimized air box with guide vane and optimized air box with bell mouth at 0.001 m valve lift until 0.008 m valve lift.	76

LIST OF SYMBOLS

h_L	Head loss
ε	Roughness
Re	Reynolds Number
K_L	Loss Coefficient
ΔP	Pressure Different
g	Constant Gravity
ρ	Density of Water
A_c	Area of The Cross Section
$\dot{m}$	Mass Flow Rate
$\dot{V}$	Volume Flow Rate
η_v	Engine Volumetric Efficiency
N	Engine Speed
D*i*	Engine Displacement
V	Velocity
Va	Engine Air Flowrate
f	Friction Factor
P_{atm}	Pressure Atmospheric
h	Elevation

LIST OF ABBREVIATIONS

AIS	Air Intake System
CFD	Computational Fluid Dynamics
3D	Three Dimensional
2D	Two Dimensional
CAD	Computer-Aided Design
SOHC	Single Over Head Cam
RPM	Revolution Per Minute

CHAPTER 1

INTRODUCTION

1.1 INTRODUCTION

The main function of an air intake system is to supply the engine with good quality of air with a correct amount to be burned inside combustion chamber. It improves the combustion efficiency and also reduces air pollution. The important characteristic on designing an intake system is its flow through the system. The flow efficiency of the intake system has a direct impact on the power the engine can deliver. Decreasing the pressure drop inside the intake system can smooth the air flow and increase the flow efficiency.

The system that cleans the air and guides it into the cylinders is called an Air Intake System (AIS). The AIS may be divided into four main parts, which are air box, intake plenum, intake manifold, and intake port. Incoming dirty air is guided into air box section where a filter is located that cleans the polluted air and other particles from entering the cylinders. Clean air then will enter the cylinders through intake plenum, intake manifold, and intake port.

In order to optimize the AIS, understanding on flows and pressure drop through the system is essential. Computational Fluid Dynamics (CFD) is considered to be the most cost-effective solution for flow analysis of the intake system.

This project will develop an optimize air box design for air intake system for Proton Waja engine. Three different design of optimize air box will be tested under various conditions of flow behavior under flow bench test and CFD analysis.

1.2 PROBLEM STATEMENT

A good quality of air increases an engine's efficiency and performance. Dirty air can damage the cylinder and shorten the engine life. Therefore, air intake system plays major role on providing clean air into the combustion chamber. Incoming dirty air is guided into the air box where a filter is located that cleans the polluted air and hinders soot and other particles before entering the combustion chamber.

Smooth air flow through the air box is important to decrease the total pressure of air entering the system. The geometry of an intake performance is related to the loss coefficient, typically identified as $K_{L,}$ which represents the fraction of the dynamic head lost in the duct. This loss can be easily controlled by proper design of the inlet duct.

Good design of air box with fewer pressure drops is one of the important thing need to figure out and studied. High pressure drop inside the intake system will cause the engine to receive improper value or air thus decreases the engine performance. An air box designed with less restriction area will smooth the air flow and reduce the pressure drop inside the system.

1.3 OBJECTIVE

Generally, the objectives to be achieved in this project are stated below:

i. To develop 3D model of an intake system.
ii. To observe the pressure drop inside the air intake system.
iii. To develop designed air box for optimization of an air intake system.

1.4 SCOPE

The project is focused on:

i. Literature review.
ii. Develop air box designs with optimum air flow.
iii. Simulate the model by using Computational Fluid Dynamic (CFD) and model test on a steady flow bench test.
iv. Result comparing and writing.

1.5 HYPOTHESIS

As the engine speed is related to the air flow rate inside the air intake system, the increment in engine speed will increase the air flow rate thus affect the flow behavior inside the intake system. As the restriction area inside the system is related to the pressure drop, wider area of restriction area will increase pressure drop for certain flow rate. As higher engine speed creates higher flow rate, the smaller restriction and smooth surface will decrease the pressure drop inside the air intake system.

1.6 METHODOLOGY

i. Stage 1 : Literature study

Make review on literature study involving project title.

ii. Stage 2 : 3D Modeling

3D modeling of the air box design

iii. Stage 3 : Boundary condition setting simulation

Set up boundary condition for simulation analysis.

iv. Stage 4 : Simulating analysis by using CFD software

Simulating analysis using FLUENT

v. Stage 5 : Model fabrication and flow bench test

Model testing on flow bench test

vi. Stage 6 : Analysis of simulation and experiment result

Analysis result from simulation and experiment

CHAPTER 2

LITERATURE REVIEW

2.1 INTRODUCTION

This chapter presents a review of literature on the efforts relating to automotive air intake system, and the pressure drop inside an air intake system. It attempts to establish what the factors are affecting the performance of intake system and how this intake system affected the car engine performance. The discussions are focused on the flow management in the intake system as a tool to optimize the air intake system. The previous study on optimization of air intake system also include in this study.

2.2 AIR INTAKE SYSTEM

The basic function of engine air intake system is to provide the engine with a fresh air-fuel mixture for combustion process inside the combustion chamber as possible (Ceviz M.A., 2010). Different engine operation requires different air intake system. In other words, a vehicle that is used for everyday purpose cannot have the same intake system as a racing vehicle. Racing engines require maximum volumetric efficiency for increase power and torque, thus the fuel consumption may increase. Daily use vehicles seldom require top-end power, thus economy and drivability at lower speeds are more important in this instance (Makgata, 2005). The air intake system development is guided by demands from

different disciplines. The requirements of each discipline itself were already taken into consideration in the past. The development of future air intake systems needs to focus on the link between the different disciplines as well (Holger, 1999).

Most of engine air intake systems consist of dirty pipe, air box, air cleaner, clean pipe, intake manifold plenum, and intake manifold runner. The length of air intake system for a car can reach up to 1 meter length. The air through these air intake systems may face great challenge of pressure drop, thus give a great challenge for induction system designer to minimize the pressure drop inside air intake system. Some important design criteria on developing intake system are low air flow resistance and good distribution of air (Ceviz, M.A, 2007). A positive pressure at the end of the frontal dirty pipe would help to overcome the drawback. Thus, most of the car manufacturer had design to put the dirty pipe at the front of the vehicle to increase the capability of the engine to consume more air from the frontal area. In fact, drawing air from the front of the vehicle can reduce the interior noise contribution from the intake orifice (Rizalman, 2008). Introduction on rib pattern inside the air box also can reduce the sound noise inside the air box and increase the part stiffness (John, 1997).

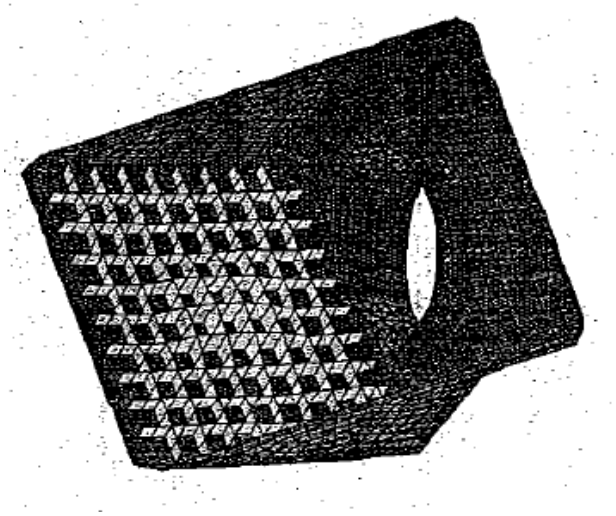

Figure 2.1: Rib pattern inside air box.

Source: John (1997)

For diesel engine, this is pretty straightforward. Air comes in the air filter housing, passes through the air filter then through the intake manifold, then the kinetic energy of the fluid resulting in turbulence causes rapid mixing of fuel and air (Murali, 2010), and is drawn into the cylinder. The most advanced part of the system was an air temperature sensor in the air intake. It was used to measure the air temperature and, by opening and closing a flap, allow cool air in through the air horn or heated air piped in from around an exhaust manifold. The reason the intake tube is long is to get the air moving in a fairly steady, coherent stream. It then passes through the air filter and then through an Air Flow Meter (Ceviz M.A., 2010)**.**

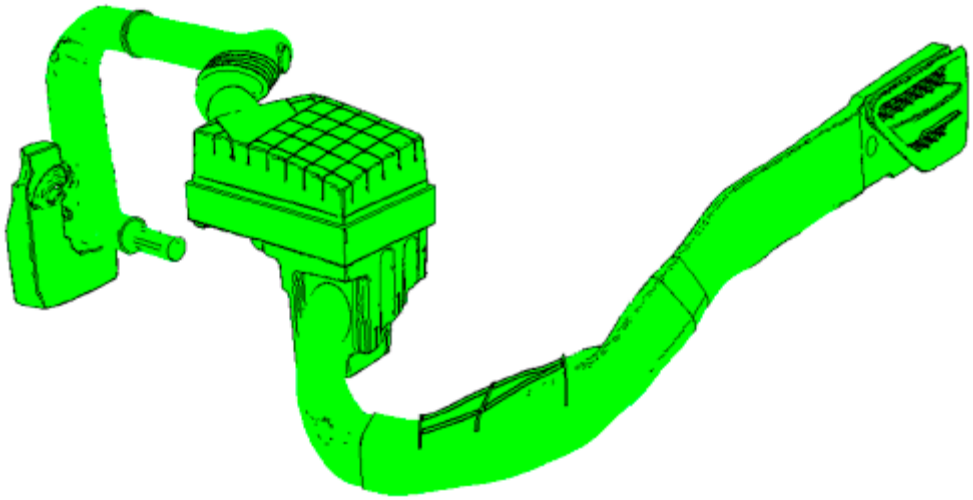

Figure 2.2: 3D geometry of air intake system.

Source: Rizalman et al (2008)

The intake system of an engine has three main functions. Its first and usually most identifiable function is to provide a clean and fresh air free from debris to the engine by method of filtering. Two other characteristics that are important for engineers to design the intake system are its flow and acoustic performance (D. Ramasamy et al, 2010) (Hyunsoo

et al, 2009). The flow efficiency of the intake system has a direct impact on the power of the engine is able to deliver. The alternating pressure induced in the induction system and in the air box causes the specific radiated sound of the whole intake system and create noise (Wolfgang, 2002). The acoustic performance is very important because it plays major role on giving noise level on vehicle during a pass-by test. Effect of adding more guide vane placement on a critical region may improve the AIS design even further (D. Ramasamy et al, 2010).

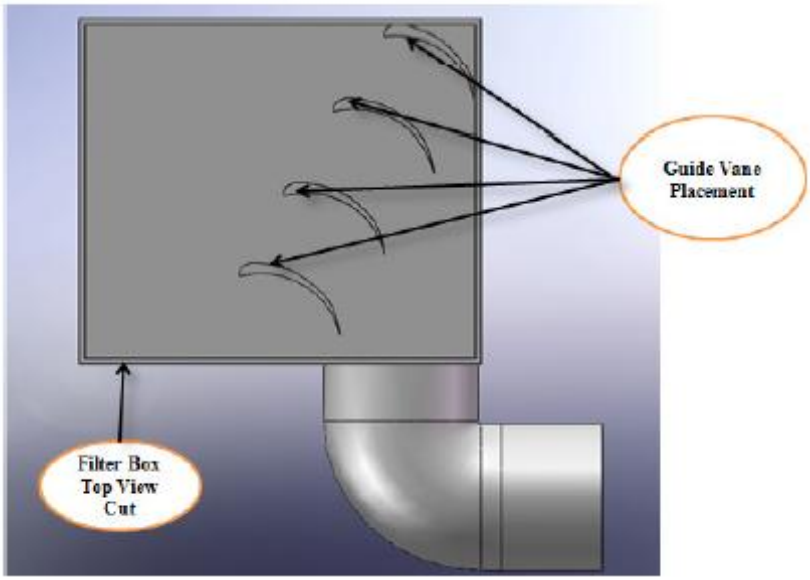

Figure 2.3: Guide vane placement by previous study.

Source: D. Ramasamy (2010)

To have effective cleaning of air from filter, it was suggested to have uniform velocity of air pass through filter (R. Yerram et al, 2006). In order to avoid the recirculation inside air box, baffle was use which would guide the flow to avoid recirculation. Baffle installation in the inlet plenum below the filter has enhanced the efficiency by guiding the flow and reducing the pressure drop significantly (R. Yerram et al, 2006) (A. Aroussi, 2003). As flow increases, pressure drop across filter bed also increases (A. S. Patil, 2005). High value of pressure drop will decrease the engine efficiency because the amount of air

supplied to the engine is not enough thus retard the combustion process. In fact, it causes more emission to occur (Rizalman et al, 2009). An uneven air distribution leads to less volumetric efficiency, power loss and increased fuel consumption (Safari et al, 2003).

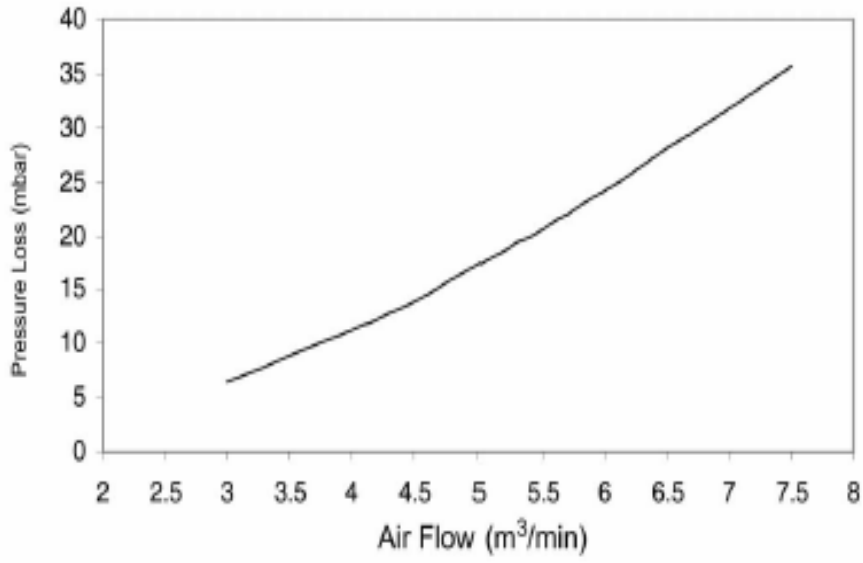

Figure 2.4: Pressure drop vs Airflow for a Typical Dry Air Filter in fresh condition

Source: A. S. Patil, (2005)

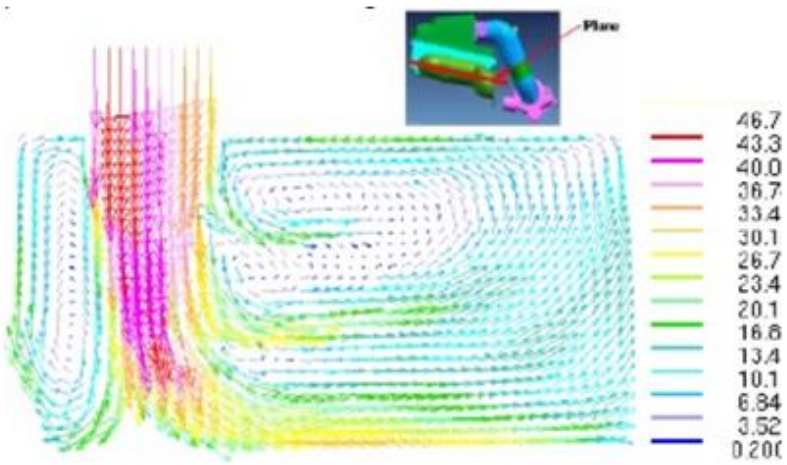

(a)

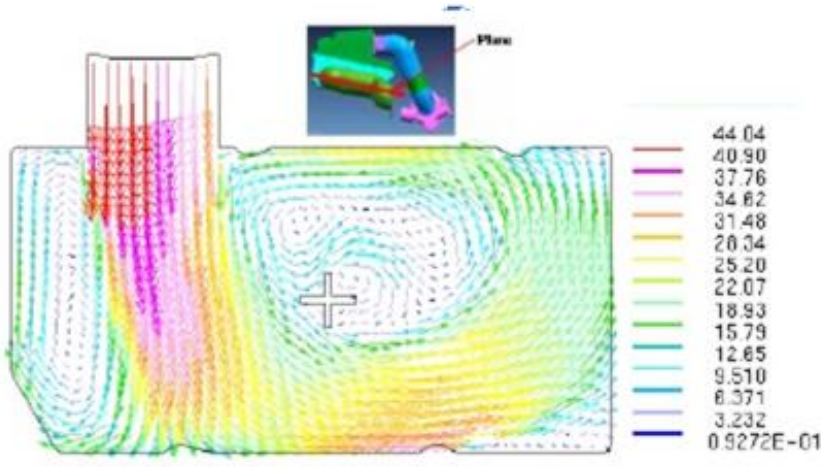

(b)

Figure 2.5: Velocity vector plot: (a) with baffle (guide vane) installation; (b) without baffle (guide vane) installation

Source: R. Yerram (2006)

Air intake systems employ specially-shaped intake tubes designed to straighten airflow as much as possible while looking great in engine compartment. These pipes are typically mandrel-bent, a process that doesn't crimp the pipe diameter at the bend. Special care is given to locating the intake tube, air box and filter in the position that best fosters maximum performance. The materials used are also selected with optimum engine conditions in mind. Near outlet plenum exit, flow was separating and recirculating at both the ends. To avoid separation and recirculation in this region, a bell-mouth was introduced (R. Yerram et al, 2006).

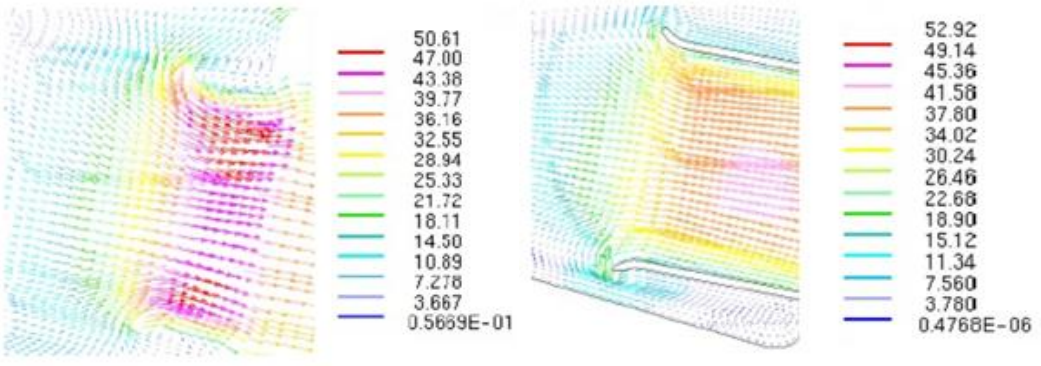

(a) (b)

Figure 2.6: Velocity vector plot: (a) near outlet without bell mouth; (b) near outlet after introducing bell mouth

Source: R. Yerram (2006)

The diameters of the air cleaner inlet and outlet tubes and connecting ducts have a major effect on the restriction of the system. The pressure drop in the ducting is inversely proportional to the fourth power of the diameter. Also, rounded elbows have much lower pressure drop than single-mitered elbows (Morton D., 1970). Corner pipe should be made smooth to avoid the reflecting shock waves that can increase the pressure drop inside the intake system (Karthikeyan, 2011) (Ravindra, 2004). The pressure drop across the air intake system can affect the indicated power of the engine. The pressure drop is created due to the suction generated by descending piston in the case of natural aspirated engine. The pressure drop along the intake system is very dependent on engine speed and load, the cross sectional area through which the fresh charge moves, and the charge density (Heywood, et al, 1988).

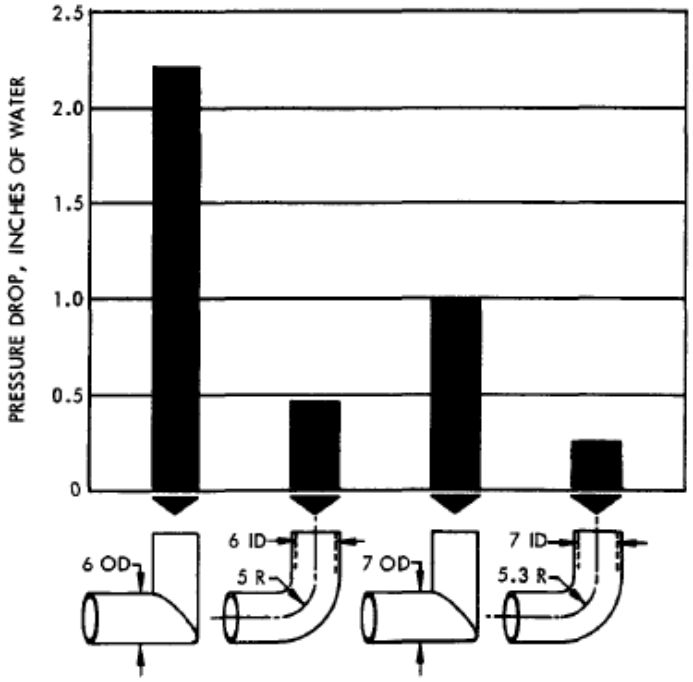

Figure 2.7: Pressure drop, single-mitered steel elbows, and curved rubber elbows at 1000 cfm.

Source: Morton D. (1970)

2.2.1 Theory of Pulsating Flow

Pulsating flow in engines is generated by piston movement during the intake cycle and by valve opening during the exhaust cycle. The type of waves that are present in engines are as follows. Sound waves occur as plane waves or spherical waves. Plane waves occur in straight pipes with constant cross sectional diameter whereas spherical waves are created by an explosion and are equal in all directions radiating from the point of explosion. A plane wave acts like a coil spring which is compressed on one side, and can be seen as it travels in the opposite direction.

Periodic waves are repeated at constant time intervals and are similar to sine waves. Waves that cause a significant displacement of the supporting gas are called finite waves which are the type of waves that are generated in engines. Their velocity is the sum of the velocities of the supporting medium and its acoustic velocity. Gas particles of compression pressure waves travel in the same direction as the wave and gas particles of expansion waves travel in the opposite direction to the expansion wave (Kriel, 2008).

2.2.2 Steady Flow Test

Steady flow bench test is widely use all over the world for most car manufacturer to study and improve the flow quality through component such as air intake system, cylinder head, and intake manifold. Much of the attention is to increase volumetric efficiency for achieving high torque and power. Test bench is equipped with measurement systems for monitoring and recording volumetric flow, speed, pressure data, and sound data (Wolfgang, 2002).

The measurement of pressure drop along the air intake system could be performed by the use of standard test bed. These measurements are carried out in complete air intake system together with cylinder head ports (Rizalman, 2008).

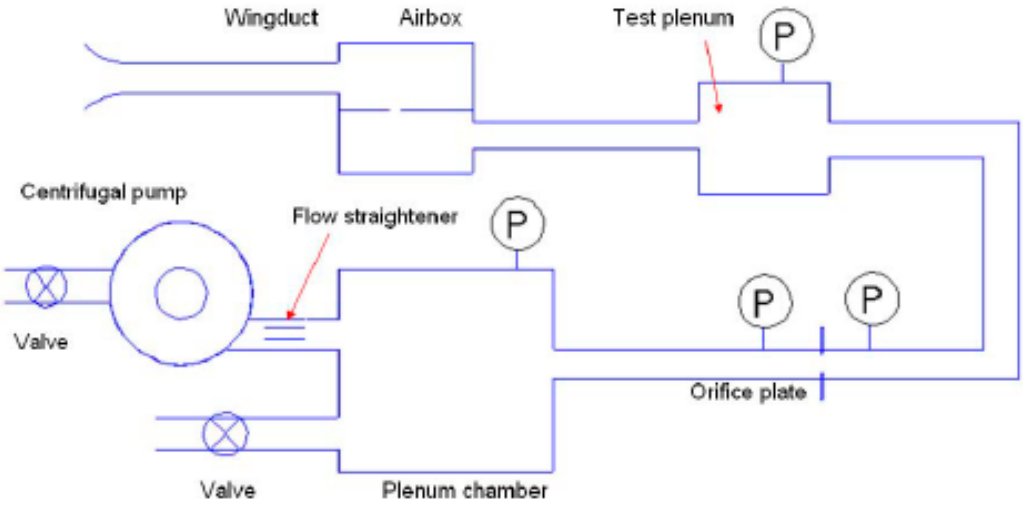

Figure 2.8: Steady flow test bench diagram

Source: Rizalman (2008)

Figure 2.8 shows the schematic arrangements of typical steady flow test bench. Essentially it consist of centrifugal fan, pressure box, air filter, valves, pipe and measurement devices such as swirl meter, flow meter, thermometer, and manometer. Advanced measurement apparatus could be used to improve understanding on air flow properties such as velocity vector and magnitude (Rizalman, 2008).

2.3 BERNOULLI EQUATION

The Bernoulli equation is a useful equation as it relates pressure changes to velocity and elevation changes along a streamline. Streamlines are lines drawn in a flow field so that at a given instant, they are tangent to the direction of the flow at every point in the flow

field. Since they are tangent to the velocity vector at every point in the flow field, there can be no flow of fluid across a streamline (Nak W. Sung. Et al 1995)

$$\frac{P_1}{\gamma} + \frac{V_1^2}{2g} + Z_1 = \frac{P_1}{\gamma} + \frac{V_2^2}{2g} + Z_2 + h_L \quad (2.1)$$

The Bernoulli equations give correct results when certain restrictions are applied.

These are as follows:

1. Steady flow

2. Incompressible flow

3. Frictionless flow

4. Flow along a streamline.

2.3.1 Major Loss

The most pipe or duct system consists of the straight pipe at this point head loss due to viscous effect Major losses, $h_{L\,major}$ can determined by equation:

$$\text{Major losses, } h_{L\,major} = f\frac{\ell}{D}\frac{V^2}{2g} \quad (2.2)$$

Friction factor, *f* to be determine using Moody chart. Using the Reynolds number and for the plastic surface of the AIS we look the graph curve at the graph smooth line (Ramasamy

et al 2010). Because the roughness, ε. For the laminar developed flow, the value of *f* is simply:

$$f = \frac{64}{Re} \tag{2.3}$$

2.3.2 Minor Loss

In the intake system, we found the system of the pipe more than a straight pipe. These additional components (valves, bends, tees, and the like) add the overall head loss of e system (Ramasamy et al 2010). Such losses are generally termed Minor losses , with the corresponding head loss denoted $h_{L\ minor}$.

$$\text{Minor losses, } h_{L\ minor} = K_L \frac{V^2}{2g} \tag{2.4}$$

The most common method used to determine these head losses or pressure drops is to specify the loss coefficient, K_L which is defined as:

$$K_L = h_{L\ minor} \cdot \frac{2g}{V^2} = \frac{\Delta p}{\frac{1}{2}\rho V^2} \tag{2.5}$$

Pressure different, ΔP*:*

$$\Delta p = K_L \frac{1}{2}\rho V^2 \tag{2.6}$$

2.3.3 Total Pressure

Total Pressure is obtained when the flowing fluid is decelerated to zero speed by a frictionless process (John, 2005). In an incompressible flow, the Bernoulli equation can be used to relate the changes in speed and pressure along a streamline for such a flow. Neglecting elevation, then equation becomes:

$$\frac{P_1}{\rho} + \frac{V_1^2}{2} = \frac{P_1}{\rho} + \frac{V_2^2}{2}$$

$$\frac{P_1}{\gamma} + \frac{V_1^2}{2g} = \text{constant} \tag{2.7}$$

If the static pressure P_1 is at a point in the flow where the speed is V_2, then the total pressure P_1, where the stagnation speed, V_1,, is zero, then the equation becomes:

$$P_1 = P_2 + \rho \frac{V_2^2}{2} \tag{2.8}$$

2.4 MASS AND VOLUME FLOW RATE

The amount of mass flowing through a cross section per unit is called the mass flow rate and its denoted by $\dot{m}$ (John, 2005). The dot over a symbol is used to indicate time rate change.

$$\dot{m} = \rho V_{avg} A_c \tag{2.9}$$

We defined the average velocity average V_{avg} value across the entire cross-section of the pipe, where A_c is the area of the cross section normal t the flow direction. The volume of the fluid flowing through a cross section per unit time is called volume flow rate, V or Q.

$$\dot{V} = V_{avg} A_c = V A_c$$

Or

$$\text{Va} = \frac{\eta_v \text{ND}i}{2} (\text{m}^3/\text{s}) \tag{2.10}$$

Where,

Va = the required engine air flowrate, m³/s

η_v = the engine volumetric efficiency (assumed 85% for normal engine specification)

N = engine speed, rpm

D*i* = engine displacement, m

The mass and volume flow rates are related by:

$$\dot{\text{m}} = \rho \dot{v} \tag{2.11}$$

2.5 COMPUTATIONAL FLUID DYNAMICS (CFD)

Computational fluid dynamics, known today as CFD, is defined as the set of methodologies that enable the computer to provide numerical simulation of fluid flows. Computational fluid dynamics is a technology that is used to analyze the dynamics of anything that can flow regardless in liquid or gaseous state. It is also a software tool that can model or simulate a flow or phenomena of any system or device under analysis (Hirsch, 2007)

CFD is computed using a set of partial different equations to predict the flow behavior. Besides that, it is also used for analyzing heat transfer model, mass flow rate, phase change, chemical reaction such as combustion, turbulence model, mechanical movement, deformation of solid structure and many more.

The word simulation is to indicate that the usage of computer in solving numerically the laws that govern the movement of fluids, in or around a material system, where its geometry is also modeled on the computer. Hence, the whole system is transformed into virtual environment or virtual product. This can be opposed to an experimental investigation, characterized by a material model or prototype of a system in measuring the flow properties in a prototype of an engine.

Simulations uses nowadays are mostly 3D simulation and 2D simulation. Both simulations differ a lot in generating data and analysis of material. 3D simulation gives the higher ability in drawing the geometrical complexity by offering un-uniform surface of a material to be simulated. This ability gives a more real-time data by creating a near real-time scenario (Hirsch, 2007). The data generated are more reliable for analysis. In contrast,

2D simulations which offer fewer geometrical complexities are mostly used to simulate a general overview of the scenario

The creation of the product is the definition phase, which covers the specification and geometrical definition. It is based on Computer-Aided Design (CAD) software, which allows creating, and defining the geometry of the system, in or its details. The CAD definition of the geometry is the required an unavoidable input to the CFD simulation task.

CFD always preferred method over the conventional design method because it is cheaper and save a lot of time. Before, there is such technology, usually engineers need to build a real model for testing and redo the model again until the optimum result is obtained. Such a long procedure would consume more money and time. With the aid of CFD software, engineer can simulate a different set of parameters for testing to get the optimum result before working on the real prototype without any additional cost (Lim, 2004).

In automotive industry for instance, the time required for the design and production of new car and engine model has been reduced from six to eight years in the 1970s to roughly 36 months in 2005, with the announced objective of 24 to 18 months in the new future. A shorter development time which is a strong demand currently from the market leads to the use of computational programs in the first concept phase (Alex M., 2001)(Negin, 2006). Thus reduce the testing cost and time (Francesco, 1995) (John, 1994) (V Ganesan, 2004). This is driven by the method known as CFD with the help of fast growing computer hardware performance (Hirsch, 2007).

One of the most important requirements before a CFD computation can be performed is the available of a suitable grid. Inability to construct a grid quickly and reliably often rules out a CFD analysis. Linear methods such as the Panel Method need

only a grid on the body surface (and road). Generation of the grid on the surface of a real vehicle to correctly capture the critical flow phenomenon is not a trivial problem. The CAD surface definition data created for body panel manufacture in the industry are helpful in generating such grids. The nonlinear CFD methods (Euler, Navier-Stokse) need a body-surrounding spatial grid to solve the partial differential equations. The inner boundary of this grid is the body surface, and the outer boundary is the bounding surface of a sufficiently large computational domain around the body.

In order to solve the Navier-Stokes equation, the flow domain for the specific problem is first discretised. Domain discretisation, using mesh or grid generation techniques, involves breaking up the selected volume into smaller volumes and solving the Navier-Stokes equation over each volume. For a simple geometry like rectangular shapes, discretisation is simple but for a complex geometry, the discretisation will become more difficult. Also, to accurately capture flow phenomena like turbulence, the grid generation must be as fine as possible to increase the number of mesh elements (Makgata, 2005). This results in a large system of non-linear equations to be calculated and require large computing memory. However, with current computing capability available today, any complex flow problems can be solved.

Commercial CFD software such as FLUENT, PHEONIX, CFX, CFD++, Star-CD, and ANSYS have been developed to a point that the user need not to be an expert on CFD in order to use the softwares. However, the user must have a good knowledge of fluid dynamics to obtain a good simulation. Therefore, used correctly, CFD software can reduce time and cost for experiments in product developement or process improvement as mention before.

2.5.1 Governing Equations

The governing equations of fluid behavior are given in equations (2.12) and (2.13) (White, 1991), (White, 1994). This equations are given for compressible flow, but also can be easily simplified for incrompressible flow too. In the Eulerian system, the particle derivative is described as follows:

$$\frac{D}{Dt} = \frac{\partial}{\partial t} + \left(\vec{V} \cdot \nabla\right) \tag{2.12}$$

where:

$$\left(\vec{V} \cdot \nabla\right) = div\vec{V} = \frac{\partial u}{\partial x} + \frac{\partial v}{\partial y} + \frac{\partial w}{\partial z}. \tag{2.13}$$

This particle derivative will be used in section to follow to present the Navier-Stokes equations in conservative form (Nak et al, 1995)(Talha et al, 2011).

2.5.2 Conservation of Mass

The equation for conservation of mass in conservation form is given as:

$$\frac{\partial \rho}{\partial t} + \nabla \cdot \left(\rho \vec{V}\right) = 0. \tag{2.14}$$

Where ρ is the density and $\vec{V}$ is the vector velocity of the fluid.

2.5.3 Conservation of Momentum

The equation for conservation of momentum in three Cartesian directions are presented.

$$\frac{\partial(\rho u)}{\partial t}+\frac{\partial\left(\rho u^{2}\right)}{\partial x}+\frac{\partial(\rho uv)}{\partial y}+\frac{\partial(\rho uw)}{\partial z}$$
$$=-\frac{\partial p}{\partial x}+\frac{\partial}{\partial x}\left(\lambda\nabla\cdot\vec{V}+2\mu\frac{\partial u}{\partial x}\right)+\frac{\partial}{\partial y}\left[\mu\left(\frac{\partial v}{\partial x}+\frac{\partial u}{\partial y}\right)\right]+$$
$$\frac{\partial}{\partial z}\left[\mu\left(\frac{\partial u}{\partial z}+\frac{\partial w}{\partial x}\right)\right]+\rho g_{x} \tag{2.15}$$

$$\frac{\partial(\rho v)}{\partial t}+\frac{\partial(\rho uv)}{\partial x}+\frac{\partial\left(\rho v^{2}\right)}{\partial y}+\frac{\partial(\rho vw)}{\partial z}$$
$$=-\frac{\partial p}{\partial y}+\frac{\partial}{\partial x}\left[\mu\left(\frac{\partial v}{\partial x}+\frac{\partial u}{\partial y}\right)\right]+\frac{\partial}{\partial y}\left(\lambda\nabla\cdot\vec{V}+2\mu\frac{\partial v}{\partial y}\right)+$$
$$\frac{\partial}{\partial z}\left[\mu\left(\frac{\partial w}{\partial y}+\frac{\partial v}{\partial z}\right)\right]+\rho g_{y} \tag{2.16}$$

$$\frac{\partial(\rho w)}{\partial t}+\frac{\partial(\rho uw)}{\partial x}+\frac{\partial(\rho vw)}{\partial y}+\frac{\partial\left(\rho w^{2}\right)}{\partial z}$$
$$=-\frac{\partial p}{\partial z}+\frac{\partial}{\partial x}\left[\mu\left(\frac{\partial u}{\partial z}+\frac{\partial w}{\partial x}\right)\right]+\frac{\partial}{\partial y}\left[\mu\left(\frac{\partial w}{\partial x}+\frac{\partial v}{\partial z}\right)\right]+$$
$$\frac{\partial}{\partial z}\left(\lambda\nabla\cdot\vec{V}+2\mu\frac{\partial w}{\partial z}\right)+\rho g_{z} \tag{2.17}$$

These equations can be rewritten as a single vector equation using indicial notation:

$$\frac{D\rho\vec{V}}{Dt} = \rho\vec{g} - \Delta p + \frac{\partial}{\partial x_j}\left[\mu\left(\frac{\partial v_i}{\partial x_j} + \frac{\partial v_j}{\partial x_i}\right) + \delta_{ij}\lambda div\vec{V}\right] \tag{2.18}$$

2.5.4 Energy Equation

The energy equation, which essence is the first law of thermodynamics, is given in its most economic form as follows:

$$\rho\frac{D}{Dt}\left(e + \frac{p}{\rho}\right) = \frac{Dp}{Dt} + div\left(k\nabla T\right) + \tau_{ij}^{'}\frac{\partial u_i}{\partial x_j} \tag{2.19}$$

Where the viscous stresses are given by the stress tensor:

$$\tau_{ij}^{'} = \mu\left(\frac{\partial u_i}{\partial x_j} + \frac{\partial u_j}{\partial x_i}\right). \tag{2.20}$$

2.5.5 Two-Equation Model: *k-ε* Model

Most of engineering flow problem in CFD simulation is turbulent. Thus it will be more complicated to solve. Turbulent flows are discribed by disordery motion of fluid in space and time. The degree of the unsteadiness of the flow is often refer to the complexity of the gemetry. Flow fluctuations bring into contact particles of differing momentum. As a result, the velocity reduce due to viscous effects; subsequently the kinetic energy is reduced (Tennekes et al, 1994). This process is said to be dissipative (Makgata, 2005).

Turbulance flow also increases the mixing of particles; thereby differing concentrations of conserved quantities are mixed. This process is called turbulent diffusion (Makgata, 2005). Turbulence depending on application for example, chemical mixing and increased wall heat transfer coefficients for better heat transfer rates than in laminar flow. In other applications, tubulence is required though it may lead to losses.

The aim of CFD is to resolve the equations that drive theoretically every kind of flow:

- The continuity equation
- The momentum equations
- The energy equation

$$\frac{\partial \rho}{\partial t} + \frac{\partial}{\partial x_k}(\rho u_k) = 0 \tag{2.21}$$

$$\frac{\partial \rho u_i}{\partial y} + \frac{\partial}{\partial x_k}(\rho u_i u_k - \tau_{ik}) + \frac{\partial P}{\partial x_i} = S_i \qquad (2.22)$$

Where ,

u = the fluid velocity,

ρ = the fluid density,

Si = a mass-distributed external force per unit mass,

E = the total energy per unit mass,

Q_H = a heat source per unit volume,

τik = the viscous shear stress tensor

qi = the diffusive heat flux.

$$\frac{\partial(\rho E)}{\partial y} + \frac{\partial}{\partial x_k}\left((\rho E + P)u_k + q_k - \tau_{ik}u_i\right) = S_k u_k + Q_H \qquad (2.23)$$

2.5.6 Model of turbulence

The turbulence modeling is significant in the internal combustion engines. In fact, turbulence directly affects the jet, the mixture homogenization and combustion in an engine (Mohamed, 2011). The adequate prediction of the turbulence behavior is necessary for a better comprehension of these phenomena in order to improve engine performances and to reduce emissions. In the majority of the multidimensional computer codes developed up to now, many key characteristics of velocity are directly related to the scales of turbulence in

the models corresponding to the admission, combustion, and transfer of heat and so on. Consequently, these processes are correctly modeled if the modeling and the prediction of turbulence are also precise. In this article, turbulence models employed for the current study will be explained according to the turbulence model k-ε (Arcoumanis, 2009). The Reynolds-stress tensor has the following form:

$$\tau_{ij}^{R} = \mu_t \left(\frac{\partial u_i}{\partial x_j} + \frac{\partial u_j}{\partial x_i} - \frac{2}{3}\delta_{ij}\frac{\partial u_k}{\partial x_k} \right) - \frac{2}{3}\rho k \delta_{ij} \tag{2.24}$$

"δ_{ij}" is equal to unity when i = j, and zero otherwise, "μ" is the dynamic viscosity coefficient, "μ_t" is the turbulent eddy viscosity coefficient and "k" is the turbulent kinetic energy. In the frame of the k-ε turbulence model, "m_t" is defined using two basic turbulence properties, namely, the turbulent kinetic energy k and the turbulent dissipation ε.

$$\mu_t = f_\mu \frac{C_\mu \rho k^2}{\varepsilon} \tag{2.25}$$

"f_μ" is a turbulent viscosity factor. It is defined by the expression:

$$f_\mu = \left(1 - e^{\left(-0{,}025\frac{\rho\sqrt{k}y}{\mu}\right)}\right)^2 \cdot \left(1 + \frac{20{,}5}{\frac{\rho k^2}{\mu\varepsilon}}\right) \tag{2.26}$$

"y" is the distance from the wall. This function allows to take into account laminar-turbulent transition. Two additional transport equations are used to describe the turbulent kinetic energy and dissipation:

$$\frac{\partial \rho k}{\partial t} + \frac{\partial}{\partial x_i}(\rho u_i k) = \frac{\partial}{\partial x_i}\left(\left(\mu + \frac{\mu_t}{\sigma_k}\right)\frac{\partial k}{\partial x_i}\right) + \tau_{ij}^R \frac{\partial u_i}{\partial x_j} - \rho\epsilon + \mu_t P_B \tag{2.27}$$

"P_B" represents the turbulent generation due to buoyancy forces and can be written as:

$$P_B = -\frac{g_i}{\sigma_B}\frac{1}{\rho}\frac{\partial \rho}{\partial x_i} \tag{2.28}$$

where "g_i" is the component of gravitational acceleration in direction x_i, the constant σ_B = 0.9

$$\frac{\partial \rho \varepsilon}{\partial t} + \frac{\partial}{\partial x_i}(\rho u_i \varepsilon) = \frac{\partial}{\partial x_i}\left(\left(\mu + \frac{\mu_t}{\sigma_\varepsilon}\right)\frac{\partial \varepsilon}{\partial x_i}\right) + C_{\varepsilon 1}\frac{\varepsilon}{k}\left(f_1 \tau_{ij}^R \frac{\partial u_i}{\partial x_j} + \mu_t C_B P_B\right) - C_{\varepsilon 2} f_2 \frac{\rho \varepsilon^2}{k} \tag{2.29}$$

"C_B" is defined as: C_B= 1 when P_B> 0, and 0 otherwise;

$$f_1 = 1 + \left(\frac{0.05}{f_\mu}\right)^3, \; f_2 = 1 - e^{\left(-\left(\frac{\rho k^2}{\mu\varepsilon}\right)^2\right)} \tag{2.30}$$

The constants C_μ, $C_{\varepsilon 1}$, $C_{\varepsilon 2}$, σ_k, σ_ε are defined empirically (Poroseva, 2001). In flow simulation the following typical values are used:

C_μ = 0:09; $C_{\varepsilon 1}$ = 1:44; $C_{\varepsilon 2}$ = 1:92; σ_k = 1; σ_ε = 1:3

2.5.7 Near-Wall Treatment

Due to the viscous and sub-layer damping effects in the turbulent boundary layer, the Reynolds number is significantly lower in this region. At high Reynolds number flows, the *k-ε* model requires a very fine grid at the turbulent boundary layer to solve for the flow properties in this region. This is due to the fact that boundary layer is very thin at high Reynolds numbers. Due to the computational effort a fine grid requires, wall functions are used near the wall.

The relations given in (2.31) are for the velocity profile in the turbulent boundary layer (Fergizer, 2002)

$$u^+ = \frac{\overline{v_t}}{u_\tau} = \begin{cases} n^+ & n^+ \le 5 \\ \frac{1}{\kappa}\ln\left(n^+\right) + B & n^+ > 30 \end{cases} \tag{2.31}$$

Where $\overline{v_t}$ is the mean velocity parallel to the wall and u_t is the shear velocity given by:

$$u_\tau = \sqrt{\frac{|\tau_w|}{\rho}} \tag{2.32}$$

Where τ_w is the shear stress at the wall, *k* is the von Karman constant (*k* = 0.41) and B is an empirical constant related to the viscous sublayer (B = 5).

In equation (2.36), n^+ is the dimensionless distance from the wall given by

$$n^+ = \frac{\rho u_\tau n}{\mu} \tag{2.33}$$

In most literature n^+ is also referred to as y^+. The log-law is valid for: 30<y^+<60.

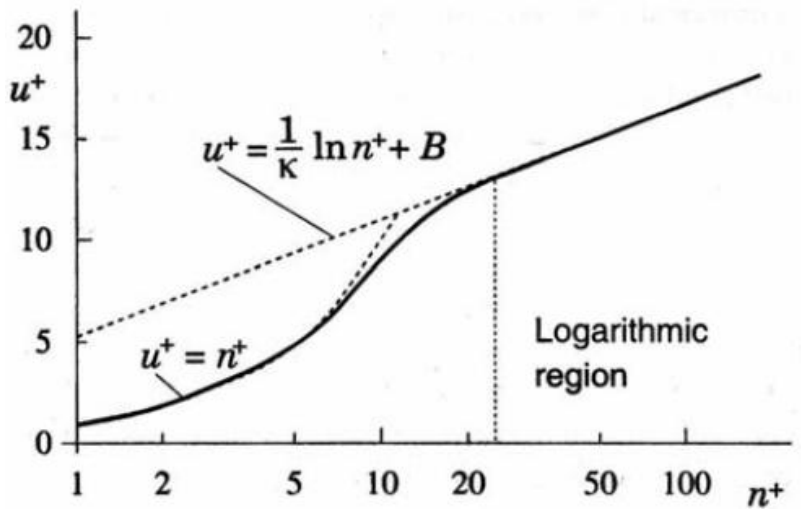

Figure 2.9: Velocity profile as function of distance normal to the wall in the turbulent boundary layer

Source: Fergizer (2002)

Figure 2.8 illustrates the velocity profile as a function of distance normal to the wall. Dashed lines are from corresponding equations whereas the solid line constitutes averaged experimental data.

2.5.8 Simulation Benefits

Technical Advantages

- Faster evaluation of new ideas, products and processes
- New insights into your process and performance
- Maximise effectiveness of your manufacturing resources
- Save time and cost, and get better results

Business Advantages

- Reduce risk and increase confidence in technical projects
- Increase customer confidence
- Increase credibility with customers
- Win more business

CHAPTER 3

METHODOLOGY

3.0 GENERAL METHODOLOGY

This chapter presents the methodology of this project. It describes on how the project is organized and steps in order to complete this project. The methodology is diverged in six parts, which are:

i. Literature study
ii. Project Flow Chart
iii. Data collecting
iv. 3D design modeling
v. Boundary condition setting simulation
vi. Meshes refinement
vii. Air flow simulation
viii. Model fabrication
ix. Flow bench test

3.1 LITERATURE STUDY

Before entering the simulation and the analysis stage, the study on the literature review is very important. The study will improve understanding of the project and gives the general idea of the project. This study will be the driven-key for the success of this project. Information from the literature study is gethered and structured into three main components below:

i. Geometry of air intake system part
ii. Effect of guide vane and bell mouth installation on air box
iii. Pressure drop in air box

3.2 FLOW CHART

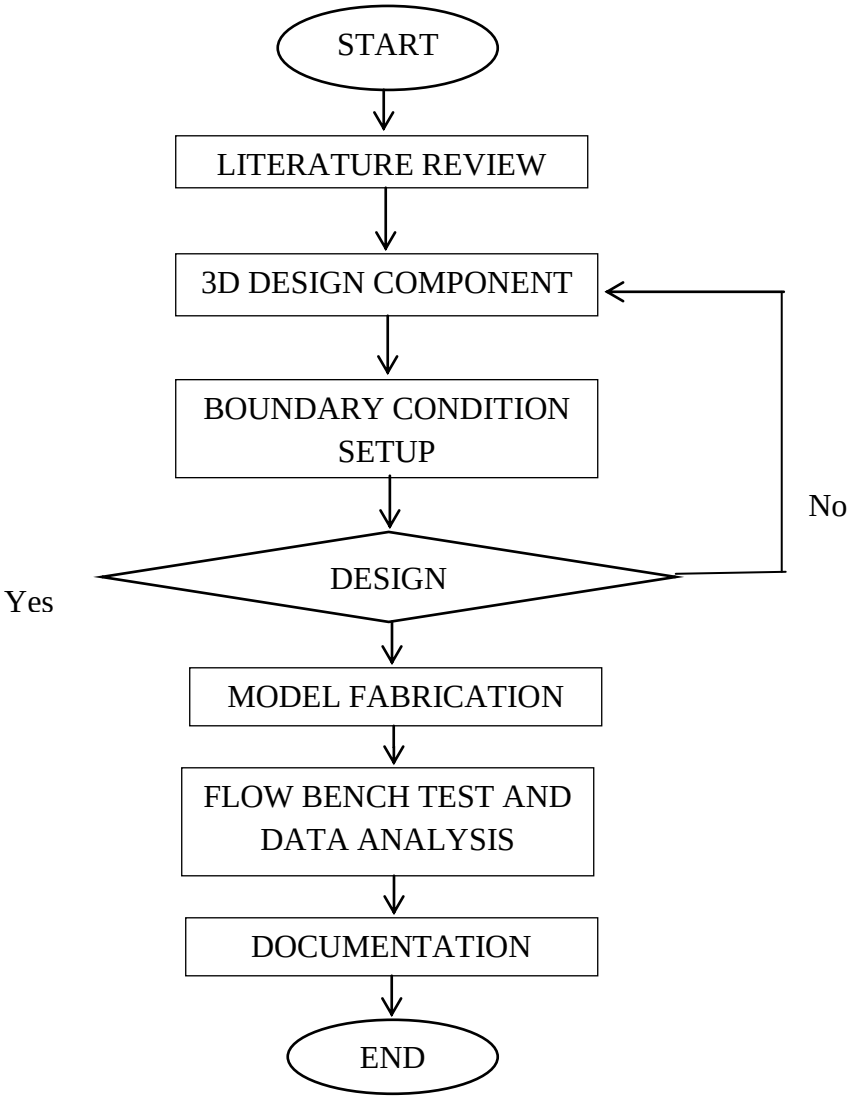

Figure 3.1: (Flow Chart)

3.3 DATA COLLECTING

Figure 3.2: Proton Waja Air Box

Proton Waja's air box was used for pattern geometry reference for design modeling. The data of the dimension for the air box was collecting from measurement then modeling the body by SolidWork software. Data collecting of dimension as accurate as possible is very important for air box to simulating the model in CFD.

To measure the area, venire caliper was used.

Inlet cross section areas = 0.003217 m^2

Outlet cross section areas = 0.004072 m^2

Thickness of plastic =0.00143 m

3.4 3D DESIGN MODELING

After measured all dimensions of the air box, the model has been design by using SolidWork software. Upper part, lower part, and filter bed have been drawn, and finally all part will assemble. Four different model was created and will be tested in CFD software to gain the optimized model. Since this study is focusing on optimization of air box by decreasing the pressure drop, rib pattern inside the air box is ignore due to neglecting the effect of sound noise and design stiffness (John, 1997).

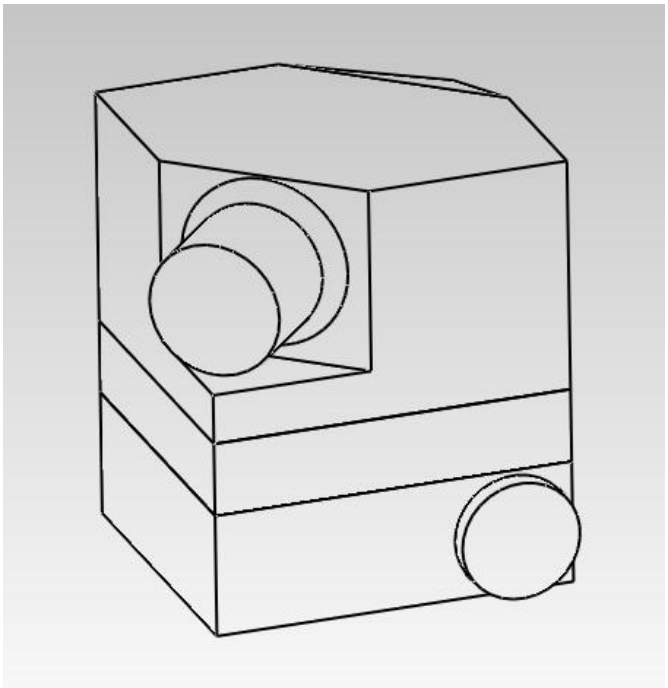

Figure 3.3: 3D Design of air box

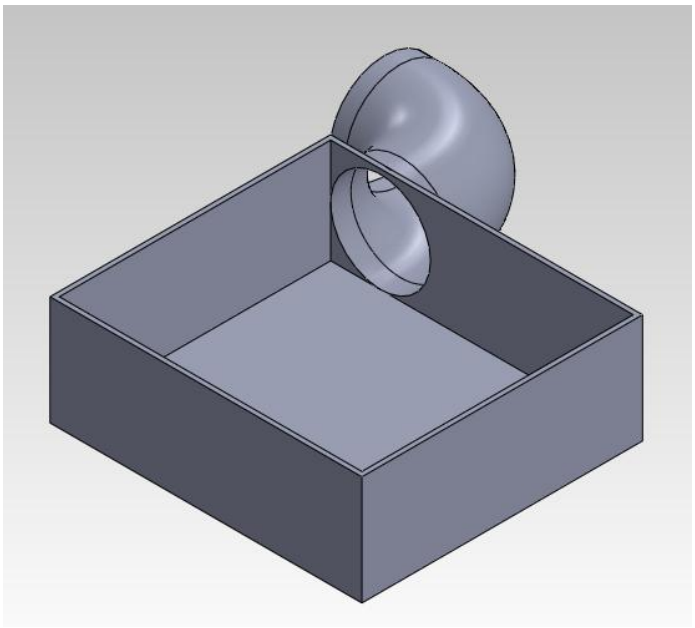

Figure 3.4: Air box lower part

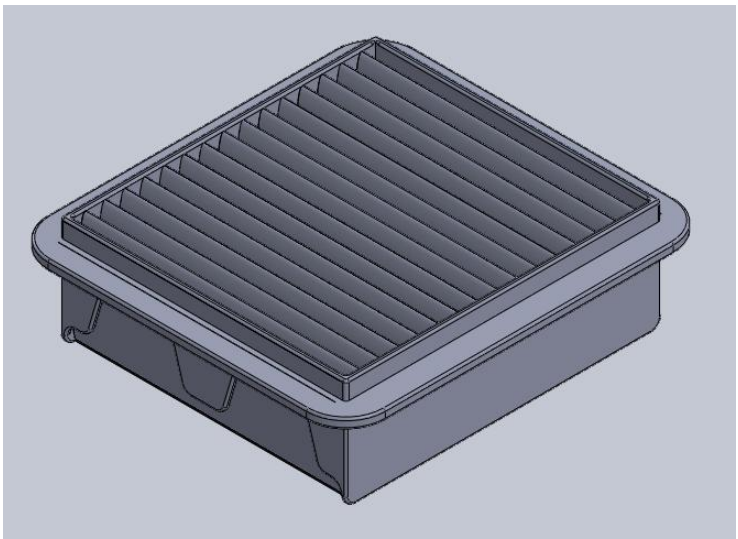

Figure 3.5: Filter bed

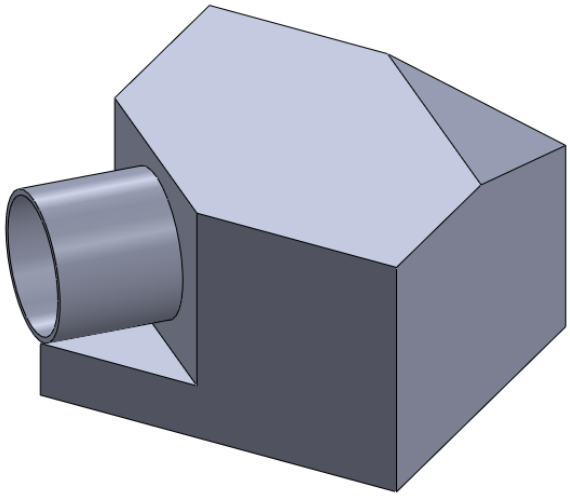

Figure 3.6: Upper part of air box

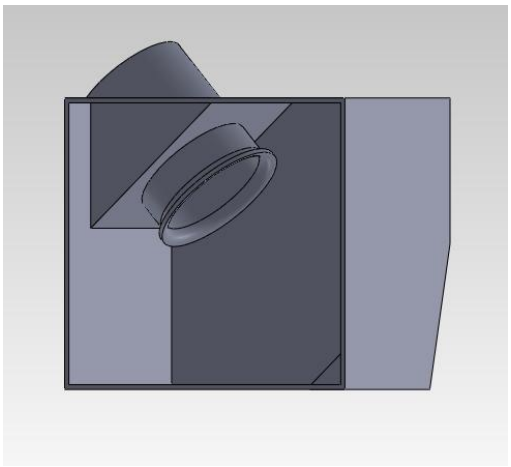

(a)

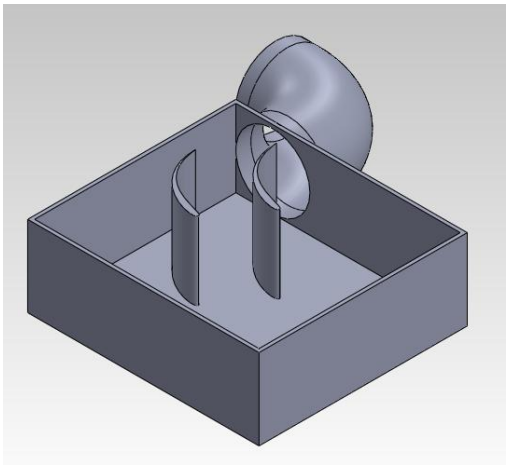

(b)

Figure 3.7: (a) Upper part air box with bell mouth, (b) Lower part air box with guide vane.

3.5 CFD SIMULATION SETUP

3.5.1 Design modeller

To identify the flow of air, a simulation tool was used. The most common educational purpose CFD ANSYS was selected for this project as the simulation tools. The ANSYS simulation simulates the flow of the air in the air box to obtain the pressure drop through the air box. The tools were also used to investigate the quality if air flow inside the air box.

The air box designs are develope using well known 3D sketching software which is SolidWork. Four different air box design model that have been created using SolidWork software are Proton Waja standard air box, Proton Waja optimized air box with guide vane and bell mouth, Proton Waja optimized air box with guide vane, and Proton Waja optimized air box with bell mouth.

Using ANSYS, selected model is being imported into design modeller to allow the geometry analysis from the model and prepare for the next step which is model meshing.

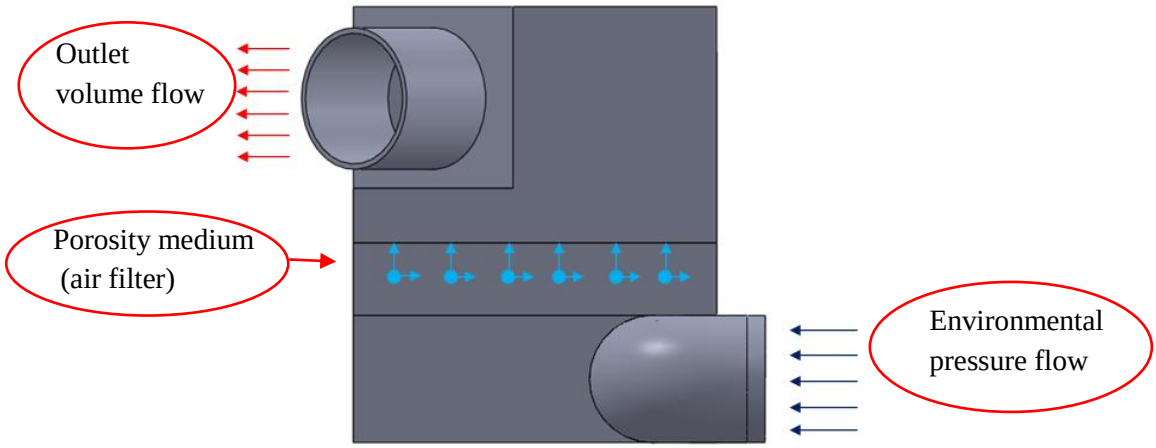

Figure 3.8: Air box in CFD model

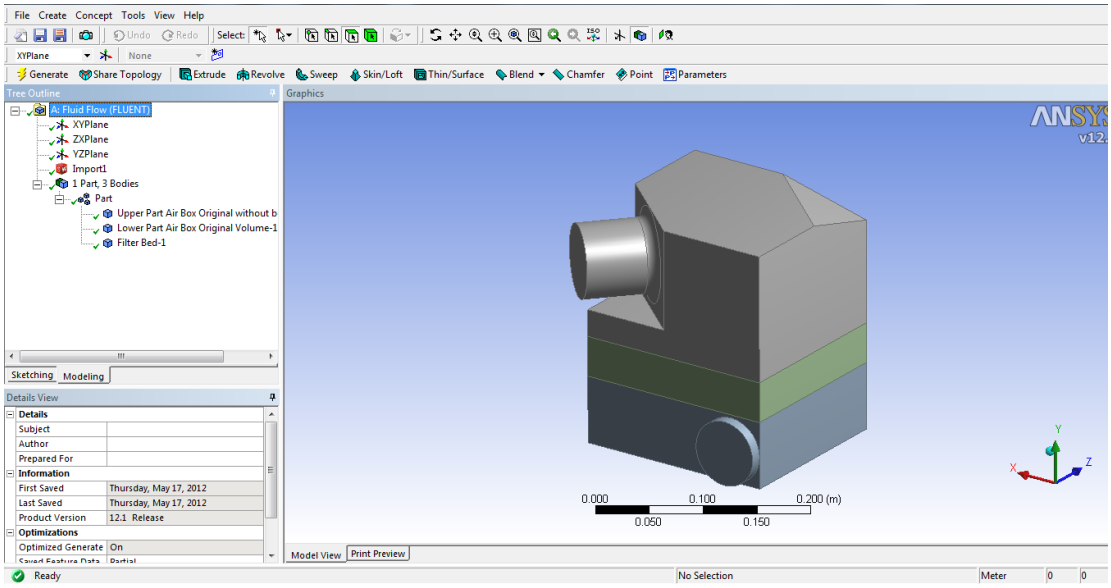

Figure 3.9: Air box in CFD design modeller

3.5.2 Computational Mesh Generation Setting

Computational mesh generation represents an important procedure in numerical analysis of complex processes. With the aid of simulation tools, one can analyze intricate flow problems. The accuracy of the numerical results is strongly influenced by the mesh mapping and the boundary conditions.

The mesh generation in the simulation tools is done automatically in solid and fluid regions eliminating the need to manually identify an optimum mesh. Automatic mesh refinement is needed in small geometric features. At first, the meshing automatically generates level three o initial mesh. Then, several identified surfaces need to have local initial mesh done due to the small gap size. If the local initial mesh is not done, the calculation on particular surfaces will be omitted, and this will affect the simulation results a lot.

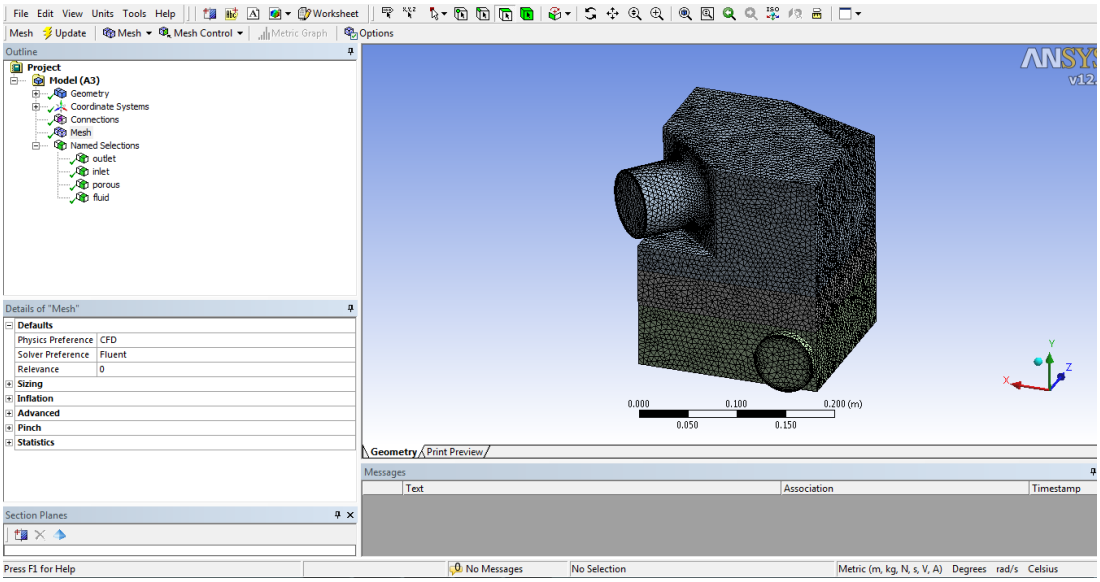

Figure 3.10: Air box in CFD meshing

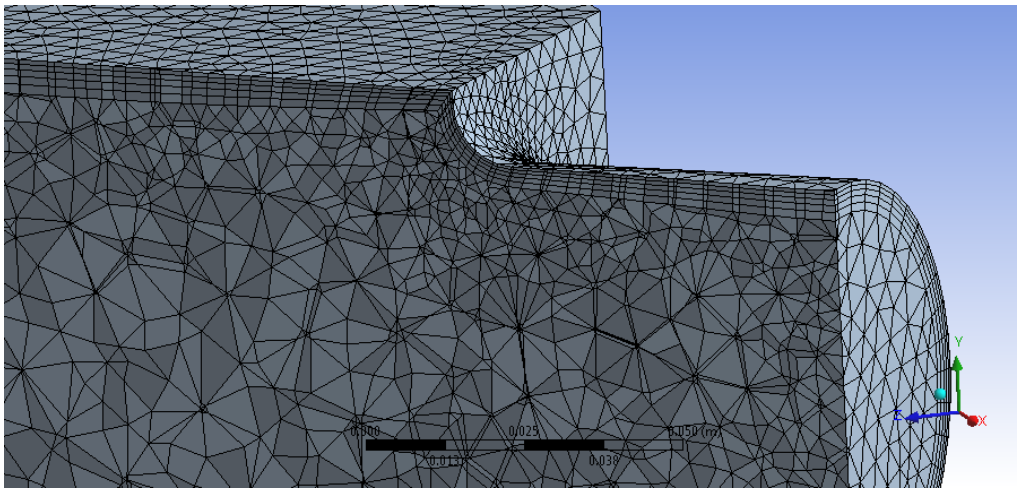

Figure 3.11: Air box mesh structure

3.5.3 Meshes Refinement

In order to get reliable and high-accuracy results, the mesh refinement method needs to be applied. Mesh refinement operation also known as volume smooth command was used to smoothes the spacing of mesh nodes throughout one or more volumes. It was applied by using smooth volume mesh from as in. While smoothing the volume mesh, the simulation tool automatically adjusts mesh node locations in order to improve the uniformity of spacing between nodes throughout the mesh.

The refinement operation and the number of refinement points are closely related in simulation time. Higher level of refinement will take longer simulation time. However, lower refinement level may cause result to be inaccurate. Time is very crucial in this project. Therefore, we need to select an appropriate refinement level by taking account the simulation time and the result accuracy. In this project level 3 of refinement level was used.

Sizing	
Use Advanced Size Function	On: Curvature
Relevance Center	Fine
Initial Size Seed	Active Assembly
Smoothing	High
Transition	Slow
Span Angle Center	Fine
Curvature Normal Angle	Default (18.0 °)
Min Size	Default (5.6286e-005 m)
Max Face Size	Default (5.6286e-003 m)
Max Tet Size	Default (1.1257e-002 m)
Growth Rate	Default (1.20)
Minimum Edge Length	2.7e-002 m

Figure 3.12: Detail of mesh sizing in AnSYS Fluent

Inflation	
Use Automatic Tet Inflation	Program Controlled
Inflation Option	Smooth Transition
Transition Ratio	0.272
Maximum Layers	5
Growth Rate	1.2
Inflation Algorithm	Pre
View Advanced Options	Yes
Collision Avoidance	Layer Compression
Fix First Layer	No
Gap Factor	0.5
Maximum Height over Base	1
Growth Rate Type	Geometric
Maximum Angle	140.0 °
Fillet Ratio	1

Figure 3.13: Detail of mesh inflation in AnSYS Fluent

3.5.4 Boundary Condition Setting Simulation

Before entering the simulation part, the boundary conditions at the design domain are established. The variables of the boundary conditions setting were clearly studied and

defined beforehand. Determining the boundary conditions is crucial because the variable setting will influence the result of the analysis. Errors in defining the boundary conditions may cause invalid simulation results.

The present problem has three types of boundaries. They are inlet, outlet and wall boundary. At the inlet, pressure boundary conditions are used to define the fluid pressure at the flow inlet. This condition is used when the inlet pressure is known but the flow rate or velocity is not known. For the outlet, velocity outlet boundary conditions require the specification of velocity at the outlet boundary. In the present case walls are assumed to be adiabatic with no slip condition. Standard wall functions are used to calculate the variables at the near wall-cells (V Ganesan, 2004).

Air was used as fluid media, which was assumed to be steady and incompressible. High Reynolds number k-ε turbulence model was used in the CFD model. CFD generally solves fluid motion by solving the Navier-Stokes equation of mass, momentum and energy equation. The three equations can be written in the conservation form as follows:

$$\frac{\partial \rho}{\partial t} + \frac{\partial}{\partial x_k}(\rho u_k) = 0 \tag{3.1}$$

$$\frac{\partial \rho u_i}{\partial y} + \frac{\partial}{\partial x_k}(\rho u_i u_k - \tau_{ik}) + \frac{\partial P}{\partial x_i} = S_i \tag{3.2}$$

$$\frac{\partial (\rho E)}{\partial y} + \frac{\partial}{\partial x_k}((\rho E + P)u_k + q_k - \tau_{ik} u_i) = S_k u_k + Q_H \tag{3.3}$$

Where,

u = the fluid velocity,

ρ = the fluid density,

S_i = a mass-distributed external force per unit mass,

E = the total energy per unit mass,

Q_H = a heat source per unit volume,

τ_{ik} = the viscous shear stress tensor and

qi = the diffusive heat flux.

The equations of mass and momentum were solved using SIMPLE algorithm to get velocity and pressure in the fluid domain. The assumption of an isotropic turbulence field used in this turbulence model was valid for the current application. The near-wall cell thickness was calculated to satisfy the logarithmic law of the wall boundary. For inlet, the outlet pressure was selected using the fixed pressure at inlet boundary condition. The value of density (1.225kg/m³), total pressure (1 atm) and turbulence intensity (5%) were specified at the inlet boundary. For outlet, outlet velocity boundary condition was set with various values of velocity based on RPM and turbulence intensity was specified as 5%. No slip boundary condition was applied on all wall surfaces. Whole domain was considered at 1 atm and at 298 K as initial condition. Other fluid properties were taken as constants. Air filter was set as porous media using coefficients. For porous media, it is assumed that, within the volume containing the distributed resistance, there exists a local balance everywhere between pressure and resistance forces such that the porosity were defined as 85%.

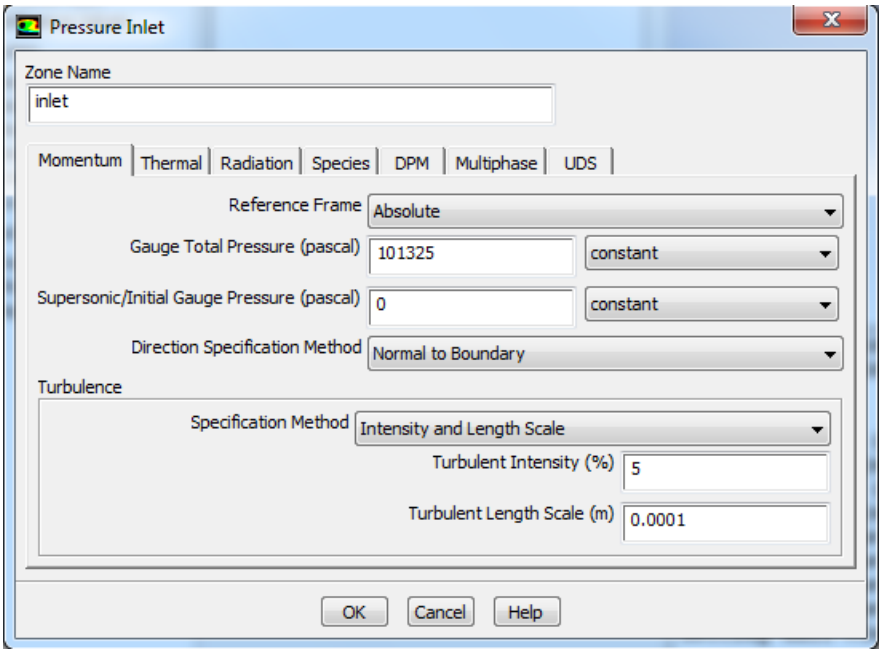

Figure 3.14: Boundary condition setting on pressure inlet for inlet zone

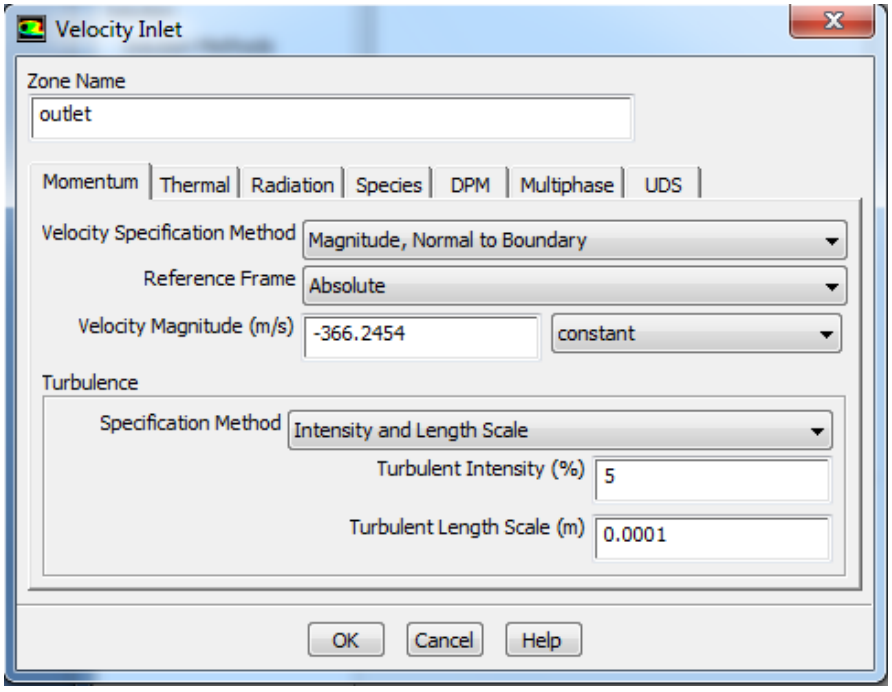

Figure 3.15: Boundary condition setting on velocity inlet for outlet zone

3.5.5 Air Flow Simulation

As the setting requirements are completed, the domain enters the simulation stage. In this stage, the process is focused on simulation tools. By using simulation tools, simple analysis could be done to measure the air flow. Additional and advanced settings are not needed during the simulation. The daya is collected when the simulation ended. The period for the simulation depends on the setting of refinement level selected.

Simulation analysis was performed on this stage after all the steps mentioned were followed. In this stage, the simulation was conducted in different engine speed state. The analysis was done with 1000 rpm increment to the maximum performance of the engine at 7000 rpm.

The simulation was done for standard air box, optimized air box with guide vane and bell mouth, optimized air box with guide vane, and optimized air box with bell mouth.

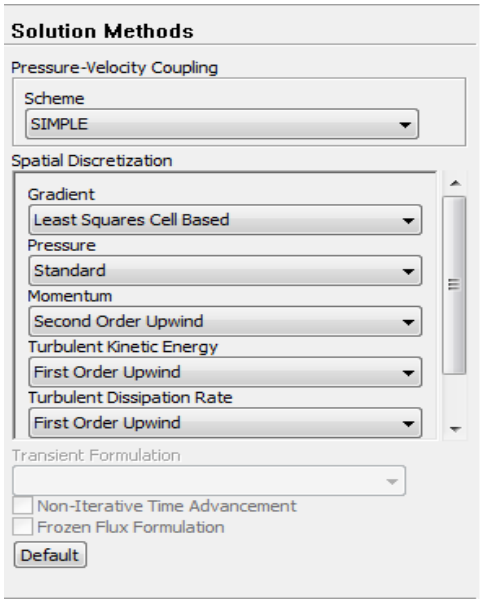

Figure 3.16: Solution method for Air box simulation

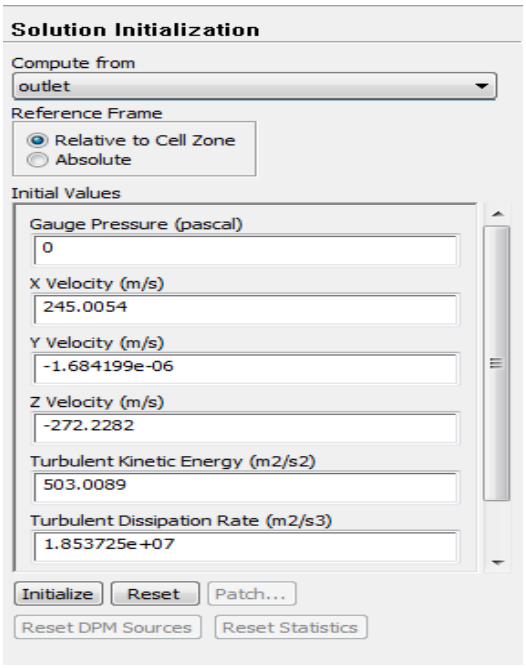

Figure 3.17: Solution initialization for Air box simulation

3.6 MODEL FABRICATION

3.6.1 Guide vane

Guide vane was made by using an aluminium plate. The shape design followed the rule of an aerodynamic aerofoil.

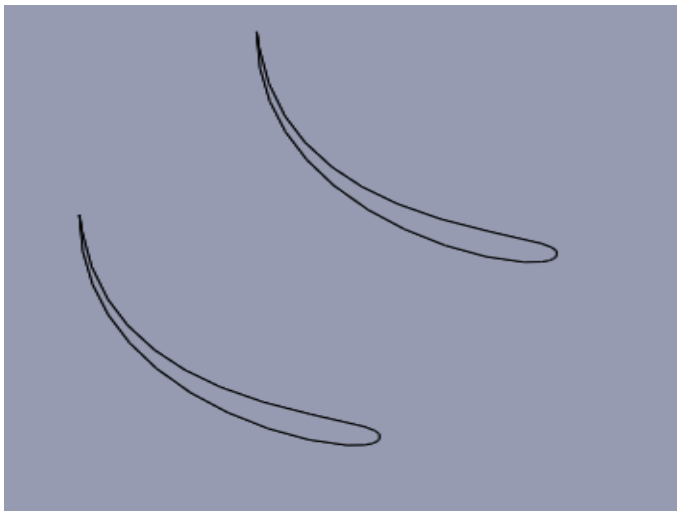

Figure 3.18: Guide vane design in SolidWork.

Figure 3.19: Fabricated guide vane.

Figure 3.20: Guide vane installation on lower part of air box

3.6.2 Bell mouth

Bell mouth was made by using an aluminium plate and after-market bell mouth of cold air intake that have been modified.

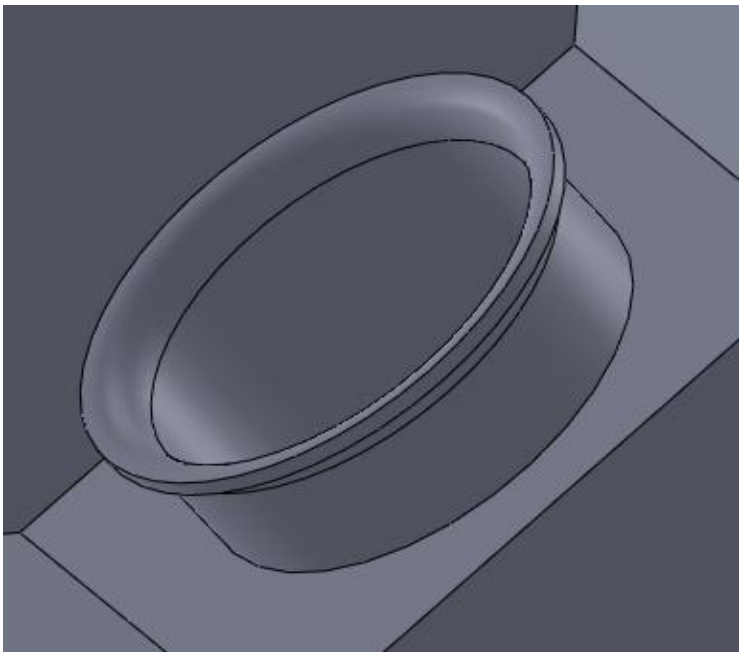

Figure 3.21: Bell mouth design on SolidWork

Figure 3.22: Fabricated bell mouth

Figure 3.23: Fabricated bell mouth installation on upper part air box

3.7 EXPERIMENTAL SETUP

The engine used was 4G18 SOHC with the number of cylinders was four. The displacement was 1584 cm^3 with a bore and stroke of 76 mm and 87.3 mm respectively. There were only four valves per cylinder, which were two for intake and another two valves for exhaust. The intake valve diameter was 26 mm. In present work, only the engine head was used.

The flow bench equipment, SuperFlow SF-1020, was used to measure the characteristics of air entering the intake manifold and combustion chamber. The flow bench consisted of an open circuit ducting system that had an air pump at the downstream to induce air flow. Pressure within the ducting system could be varied by changing the speed of the air pump. The flow bench equipment setting is shown in Figure 3.15. The engine's cylinder head with complete valves assembly was attached to a head adapter, which

resembled the engine's cylinder, at the top of the bench. A dial gauge was mounted at the top of the intake valve to enable precision variation of the valve lifts. The calibrated dial gauge is used to adjust the valve lift (Vinodh et al, 2010).The intake manifold was attached to the engine head with gasket to seal the air from leakage. The specifications of the flow bench system are shown in Table 3.1 (Ismail et al., 2008).

Figure 3.24: Cylinder head setting on head adapter on flow bench test

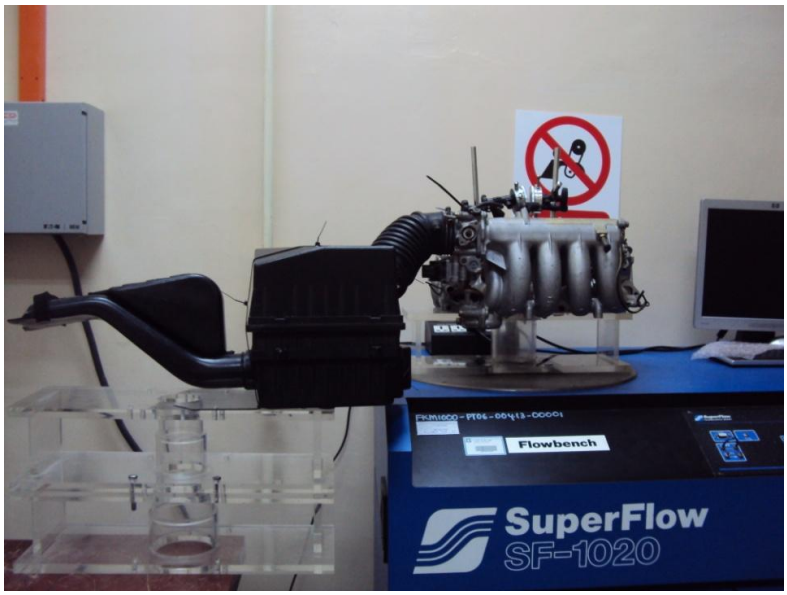

Figure 3.25: Air box setting on flow bench test

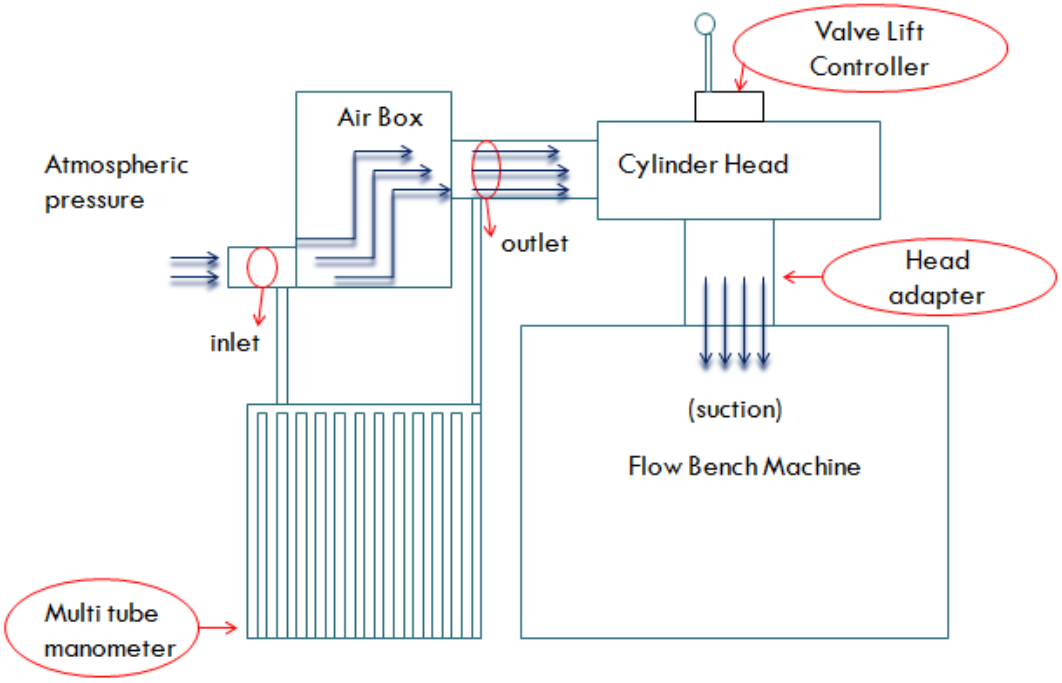

Figure 3.26: Air box setting on flow bench test diagram

Table 3.1: Specifications of flow bench system

Source: SF-1020 Flowbench Operator's Manual

Parameter	Value
Make and model	SuperFlow, SF-1020
Flow measurement accuracy:	±0.05%
Flow repeatability:	±0.25%
Flow range:	12 - 470 l/s
Pressure accuracy:	± 0.13 cm of water
Pressure range:	0 - 165 cm of water
Temperature accuracy:	±0.3˚C

In the experiments, only the intake valve lift was varied, while the exhaust valves remained close at all time. The intake valve was lifted, from fully closed position, at an increment of one millimeter to a maximum lift of eight milimeter (S. A. Sulaiman, 2010).

Universal test pressure which was 25cmH_2O was set in this experiment. The pressure drop was measured by manometer (Athanasios, 1999).The value of height, h, at inlet and outlet on the manometer was recorded for each valve lift.

Figure 3.27: Multitube Manometer model SOLTEQ FM21-VT-A

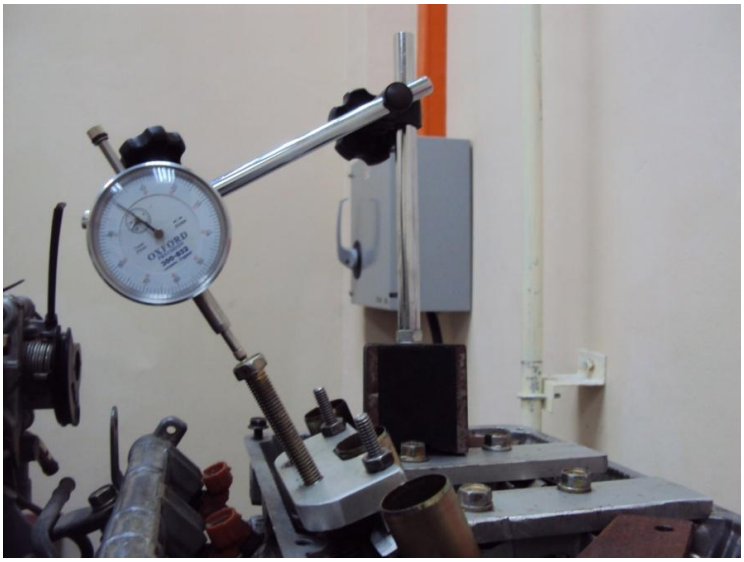

Figure 3.28: Dial gauge on valve lift controller; model OXFORD 300-852

CHAPTER 4

RESULTS AND DISCUSSIONS

4.1 INTRODUCTION

This chapter will discuss the result of analysis on two different designs of the air box that have been conducted using CFD analysis and flow bench test, which are standard part and optimized part with guide vane and bell mouth. The calculation on inlet and outlet surface of a testing model is taken, which is the dynamic pressure. Then, the pressure different between the inlet and outlet were calculated.

4.2 CALCULATION OF AIR VELOCITY

In order to define the air velocity through the air box for certain engine RPM, the calculation of volume flow rate is applied. Volume flow rate, Va is defined as

$$\text{Va} = \frac{\eta_v \text{ND}i}{2} (\text{m}^3/\text{s})$$

Where,

Va = the required engine air flowrate, m^3/s

η_v = the engine volumetric efficiency (assumed 85% for normal engine specification)

N = engine speed, rpm

D*i* = engine displacement, m^3 ($6.6348x10^{-3}m^3$)

The mass flow rate and volume flow rate are related by:

$$\dot{m} = \rho \dot{v}$$

Where,

$\dot{m}$ = mass flow rate (kg/s)

ρ = Air density (1.225 kg/m^3)

$\dot{v}$ = Volume flow rate (m^3/s)

The velocity and volume flow rate are related by:

$$\dot{v} = AV$$

Where,

$\dot{v}$ = Volume flow rate (m^3/s)

A = Area (m^2)

V = Velocity (m/s)

The result for mass flow rate and volume flow rate for each RPM will be analyzed here. The value of volume flow rate will be use to measure the value of velocity at the outlet.

Table 4.1: Table of volume flow rate (m^3/s), mass flow rate (kg/s), and outlet velocity (m/s) for 1000 RPM until 7000 RPM.

RPM	Air Density (kg/m^3)	Volume Flow Rate (m^3/s)	Mass Flow Rate (kg/s)	Outlet Velocity (m/s)
1000	1.225	0.1683	0.2062	41.33
2000	1.225	0.3366	0.4124	82.67
3000	1.225	0.5049	0.6185	124.00
4000	1.225	0.6733	0.8247	165.34
5000	1.225	0.8416	1.0309	206.67
6000	1.225	1.0099	1.2371	248.01
7000	1.225	1.1782	1.4433	289.34

(Calculation for RPM = 3000)

Volume flow rate, Va $= \frac{\eta_v N D i}{2}$

$= \frac{(0.85)(3000)(6.6348 \text{x} 10^{-3}\ m^3)}{2}$

$= 0.5049\ m^3/s$

Mass flow rate, ṁ $= \rho \dot{v}$

$= (1.225)(0.5049)$

$= 0.6185$ kg/s

Velocity, V $= \frac{\dot{v}}{A}$

$= \frac{0.5049\ (m^3/s)}{0.004072\ (m^2)}$

$= 124.00$ (m/s)

4.3 RESULTS

4.3.1 CFD Simulation result

The results of CFD analysis for standard and optimized air box have been obtained and will be analyzed in this section.

Table 4.2: Result of pressure drop for CFD analysis on standard air box at 1000 RPM until 7000 RPM

RPM	Air density, kg/m³	Volume flow rate, m³/s	Mass flow rate, kg/s	Inlet pressure, Pa	Outlet pressure, Pa	Pressure drop ΔP, Pa
1000	1.225	0.1683	0.2062	1555.54	1058.11	497.43
2000	1.225	0.3366	0.4124	6217.06	4229.02	1988.04
3000	1.225	0.5049	0.6185	14715.49	9510.36	5205.13
4000	1.225	0.6733	0.8247	25181.20	16903.55	8277.65
5000	1.225	0.8416	1.0309	39821.72	26425.23	13396.49
6000	1.225	1.0099	1.2371	55544.51	38052.07	17492.44
7000	1.225	1.1782	1.4433	75634.00	51786.89	23847.11

Table 4.3: Result of pressure drop for CFD analysis on optimized air box (Guide vane and bell mouth) at 1000 RPM until 7000 RPM

RPM	Air density, kg/m³	Volume flow rate, m³/s	Mass flow rate, kg/s	Inlet pressure, Pa	Outlet pressure, Pa	Pressure drop ΔP, Pa
1000	1.225	0.1683	0.2062	1693.19	1196.65	496.53
2000	1.225	0.3366	0.4124	6621.82	4375.06	2246.77
3000	1.225	0.5049	0.6185	14958.59	10055.66	4902.93
4000	1.225	0.6733	0.8247	26402.90	18189.96	8212.95
5000	1.225	0.8416	1.0309	41175.82	28638.55	12537.28
6000	1.225	1.0099	1.2371	59551.48	41448.10	18103.39
7000	1.225	1.1782	1.4433	79788.59	56865.58	22923.01

Table 4.4: Result of pressure drop for CFD analysis on optimized air box (Guide vane only) at 1000 RPM until 7000 RPM

RPM	Air density, kg/m³	Volume flow rate, m³/s	Mass flow rate, kg/s	Inlet pressure, Pa	Outlet pressure, Pa	Pressure drop ΔP, Pa
1000	1.225	0.1683	0.2062	1665.55	1102.09	563.46
2000	1.225	0.3366	0.4124	6652.37	4260.94	2391.43
3000	1.225	0.5049	0.6185	14906.72	9589.04	5317.68
4000	1.225	0.6733	0.8247	26438.65	17024.11	9414.54
5000	1.225	0.8416	1.0309	41686.24	26581.47	15104.77
6000	1.225	1.0099	1.2371	59561.27	38236.79	21324.47
7000	1.225	1.1782	1.4433	80794.75	51986.95	28807.80

Table 4.5: Result of pressure drop for CFD analysis on optimized air box (Bell moth only) at 1000 RPM until 7000 RPM

RPM	Air density, kg/m³	Volume flow rate, m³/s	Mass flow rate, kg/s	Inlet pressure, Pa	Outlet pressure, Pa	Pressure drop ΔP, Pa
1000	1.225	0.1683	0.2062	1599.72	1147.87	451.86
2000	1.225	0.3366	0.4124	6353.78	4587.11	1766.67
3000	1.225	0.5049	0.6185	14307.45	10337.52	3969.93
4000	1.225	0.6733	0.8247	25237.73	18367.73	6870.00
5000	1.225	0.8416	1.0309	38698.15	28699.48	9998.68
6000	1.225	1.0099	1.2371	58424.38	41320.84	17103.55
7000	1.225	1.1782	1.4433	78343.44	56245.25	22098.19

The curve for pressure drop with point was plotted to see the difference between the pressure drop at each RPM for standard air box part, optimized air box part with guide vane, optimized air box part with bell mouth, and optimized air box part with guide vane and bell mouth respectively. Figure 4.1, 4.2, 4.3, 4.4, 4.5, and Figure 4.6 show the comparison of pressure drop between the air box parts from 1000 RPM until 7000 RPM.

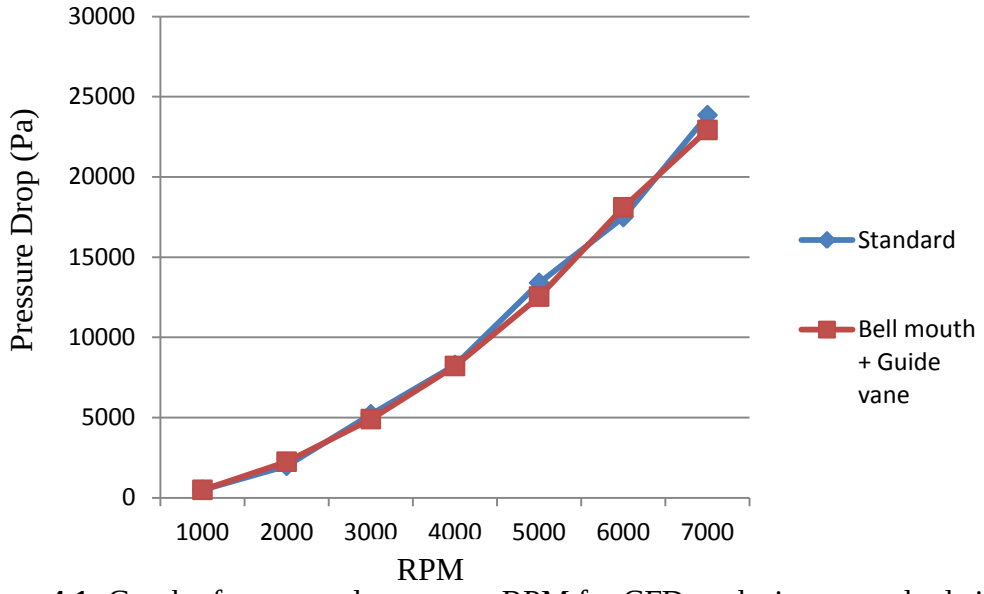

Figure 4.1: Graph of pressure drop versus RPM for CFD analysis on standard air box and optimized air box with guide vane and bell mouth at 1000 RPM until 7000 RPM

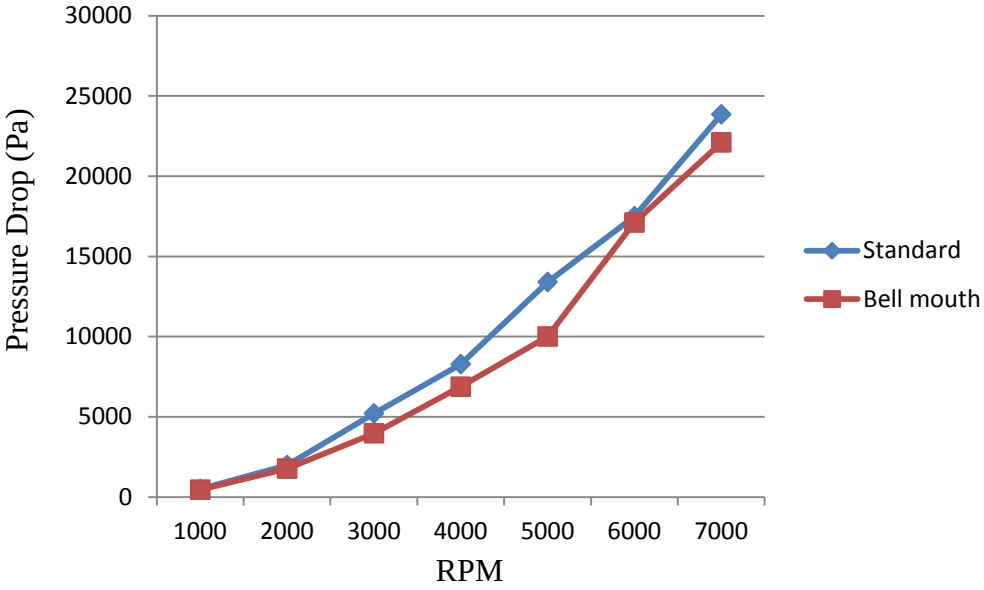

Figure 4.2: Graph of pressure drop versus RPM for CFD analysis on standard air box and optimized air box with bell mouth at 1000 RPM until 7000 RPM

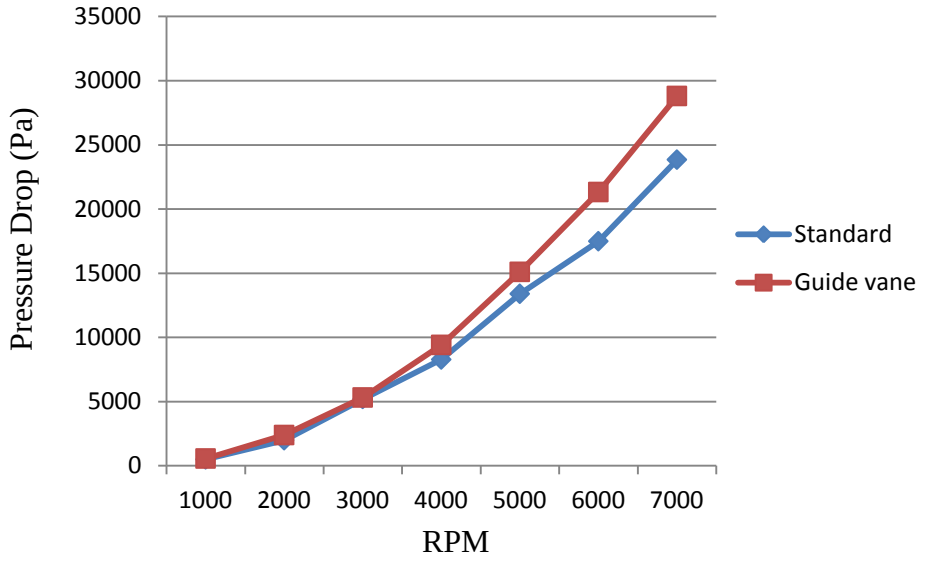

Figure 4.3: Graph of pressure drop versus RPM for CFD analysis on standard air box and optimized air box with guide vane at 1000 RPM until 7000 RPM

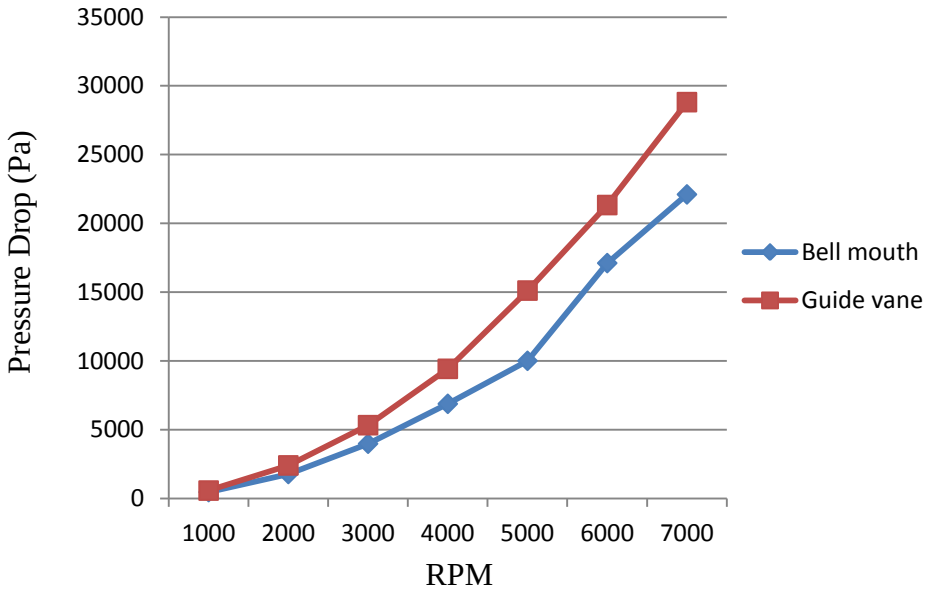

Figure 4.4: Graph of pressure drop versus RPM for CFD analysis on optimized air box with bell mouth and optimized air box with guide vane at 1000 RPM until 7000 RPM

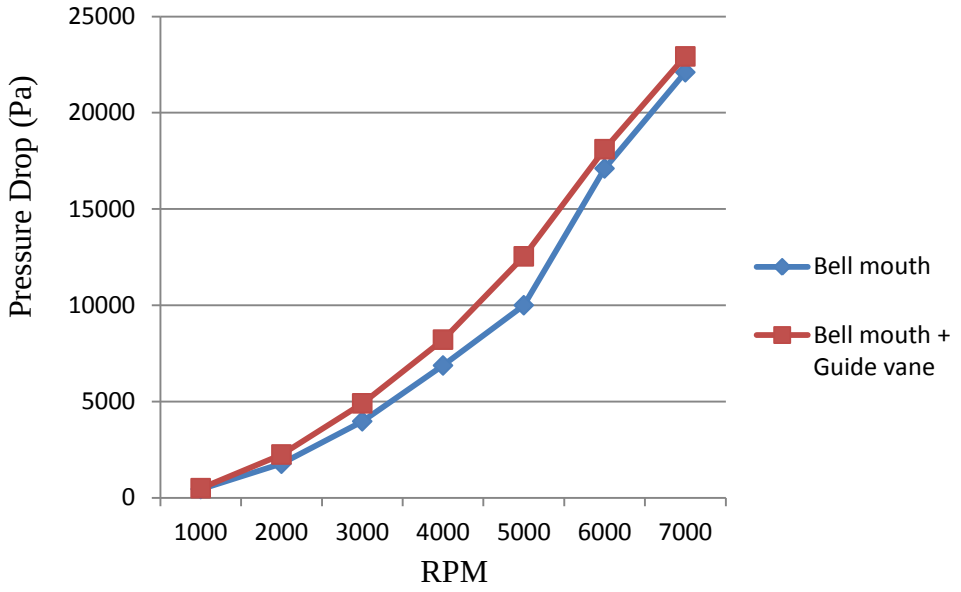

Figure 4.5: Graph of pressure drop versus RPM for CFD analysis on optimized air box with bell mouth and optimized air box with bell mouth and guide vane at 1000 RPM until 7000 RPM

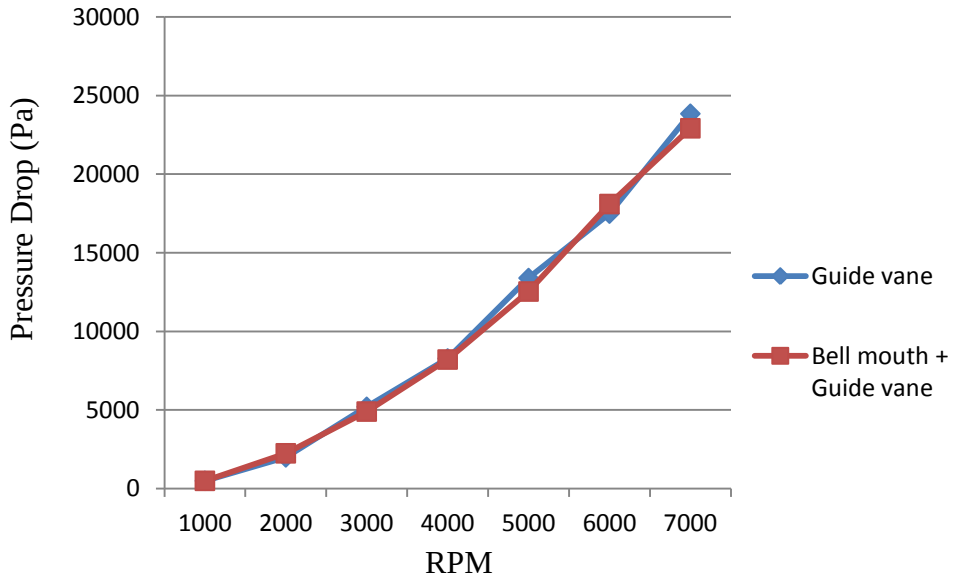

Figure 4.6: Graph of pressure drop versus RPM for CFD analysis on optimized air box with guide vane and optimized air box with bell mouth and guide vane at 1000 RPM until 7000 RPM

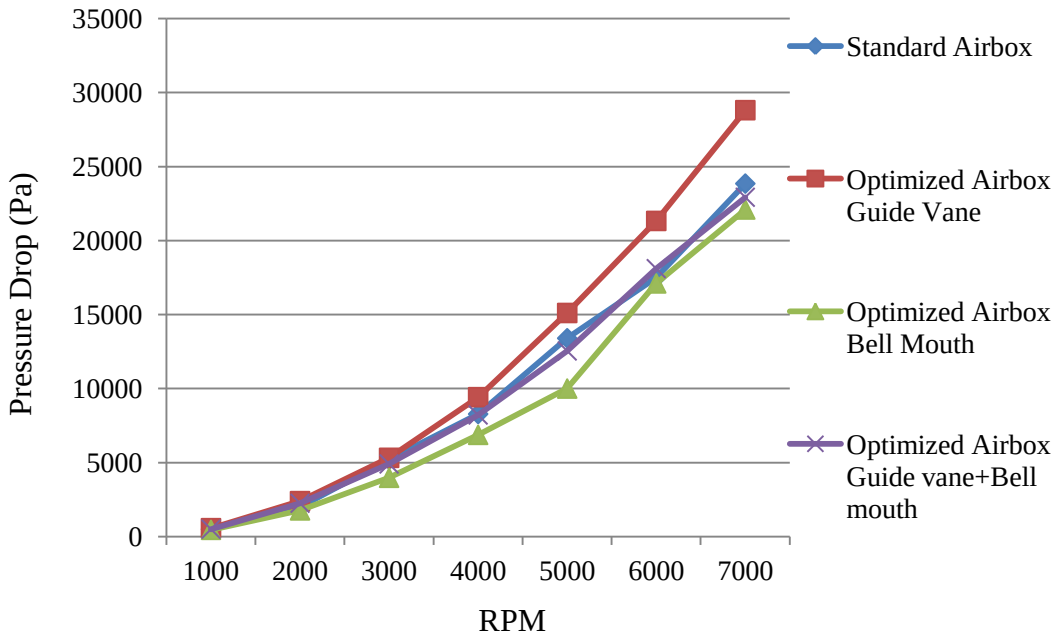

Figure 4.7: Graph of pressure drop versus RPM for CFD analysis on standard air box, optimized air box with bell mouth, optimized air box with guide vane, and optimized air box with bell mouth and guide vane at 1000 RPM until 7000 RPM

From the CFD analysis, velocity magnitude (m^2/s) contour plot of air box parts was extracted to see the flow velocity for standard air box and optimized air box. Figure 4.7, 4.8, 4.9, 4.10, 4.11, 4.12, 4.13, and Figure 4.14 show the contour plot of velocity magnitude (m^2/s) for standard air box and optimized air box at 4000 RPM.

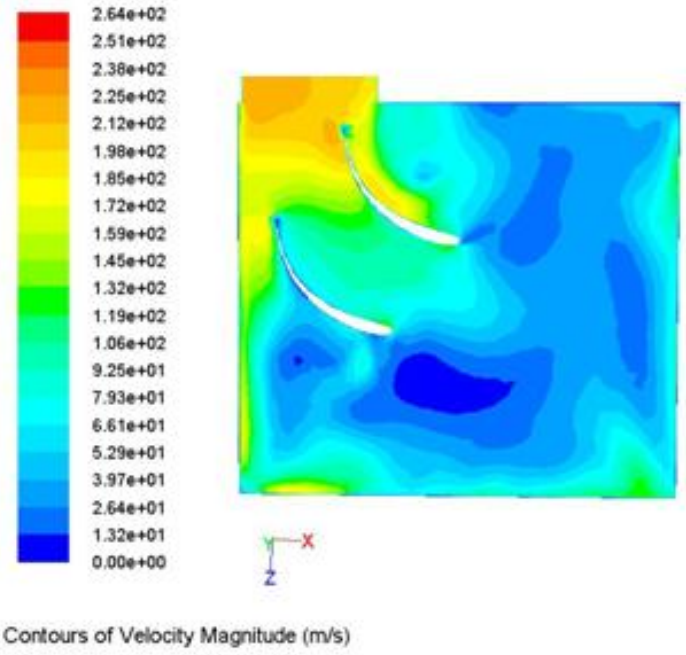

(a)

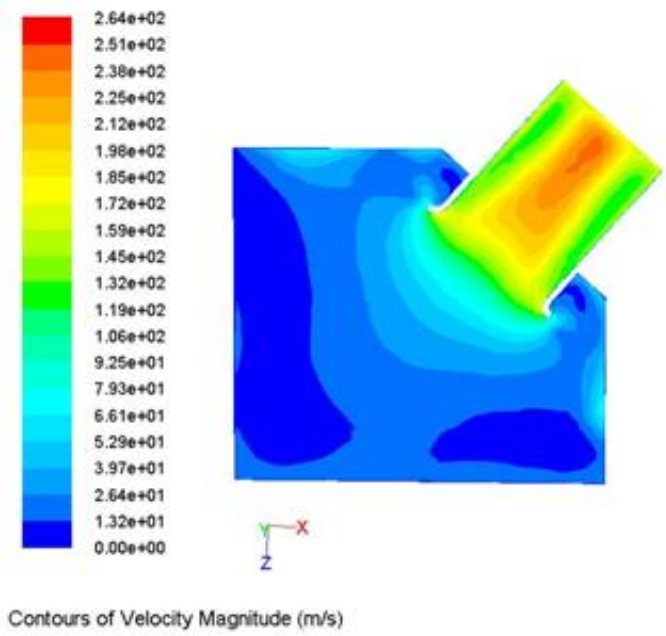

(b)

Figure 4.8: Velocity magnitude (m^2/s) contour plot: (a) lower part optimize air box with bell mouth and guide vane; (b) upper part optimize air box with bell mouth and guide vane

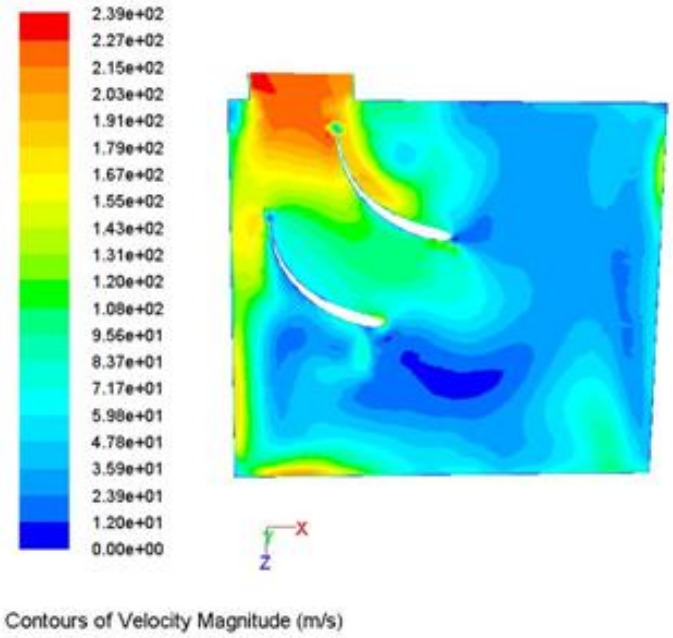

(a)

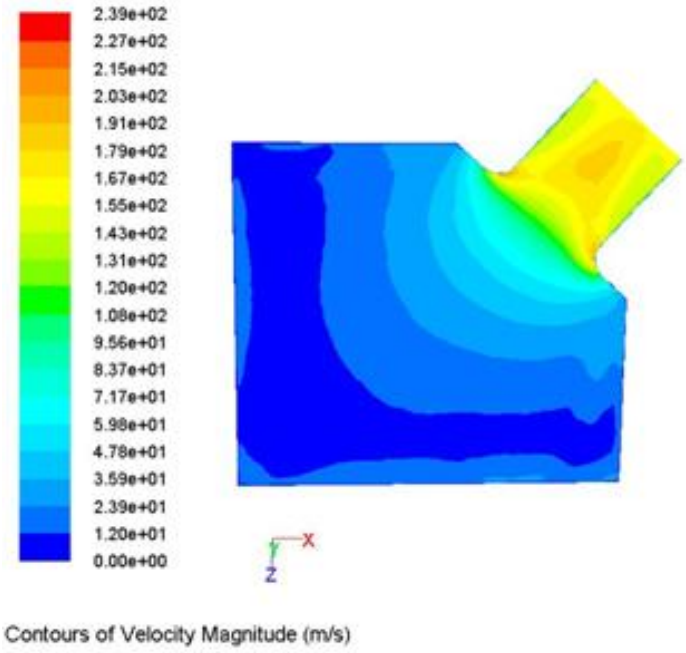

(b)

Figure 4.9: Velocity magnitude (m^2/s) contour plot: (a) lower part optimize air box with guide vane; (b) upper part optimize air box with guide vane

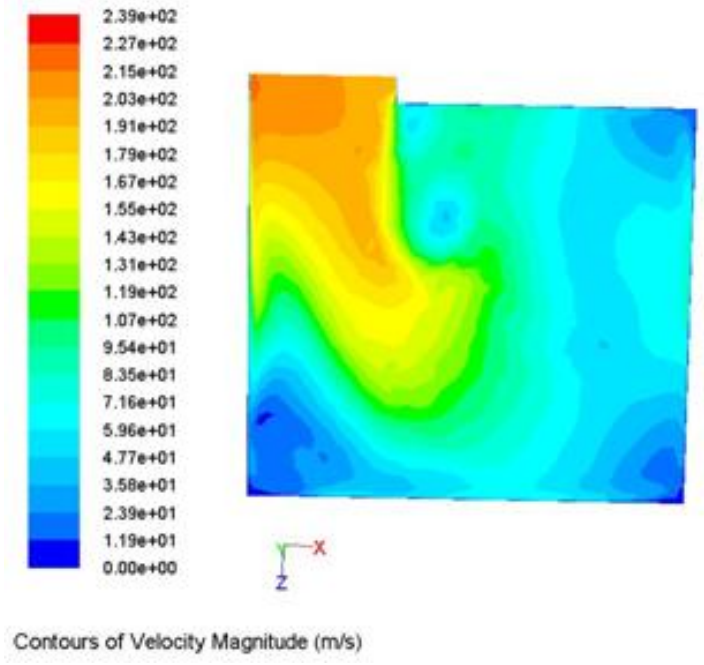

(a)

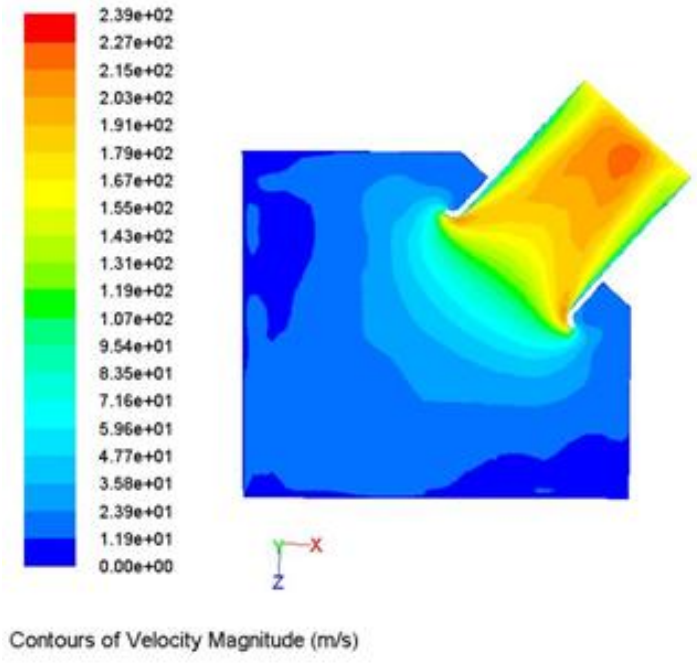

(b)

Figure 4.10: Velocity magnitude (m²/s) contour plot: (a) lower part optimize air box with bell mouth; (b) upper part optimize air box with bell mouth

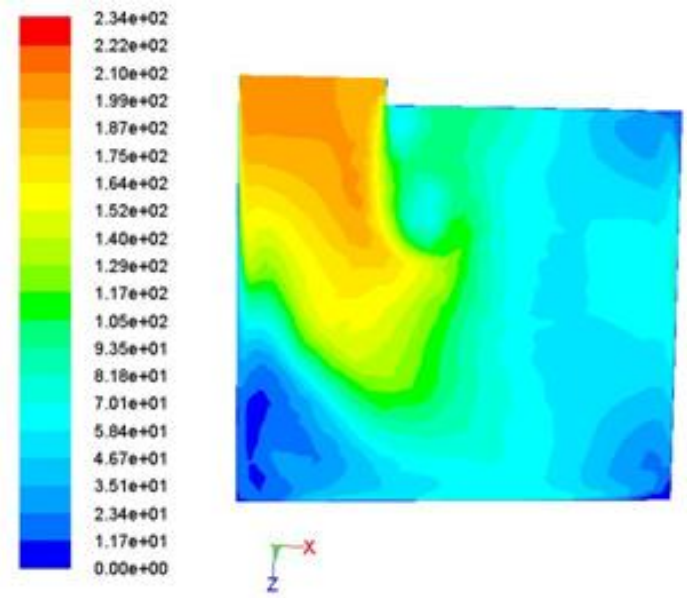

(a)

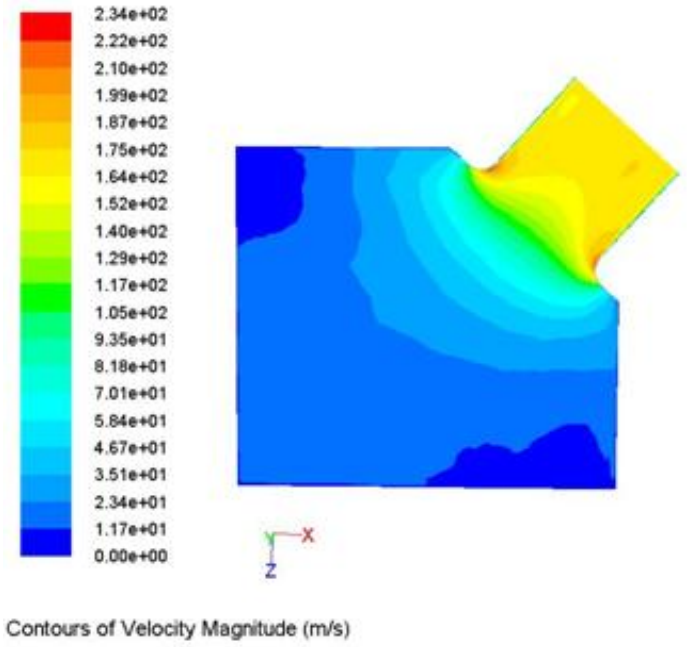

(b)

Figure 4.11: Velocity magnitude (m^2/s) contour plot: (a) lower part standard air box; (b) upper part standard air box

From the CFD analysis, velocity magnitude (m^2/s) vector plot of air box parts was extracted to see the vector velocity track for standard air box design and optimized air box design. Figure 4.11 and Figure 4.12 show the vector plot of velocity magnitude (m^2/s) for standard air box design and optimized air box design at 4000 RPM.

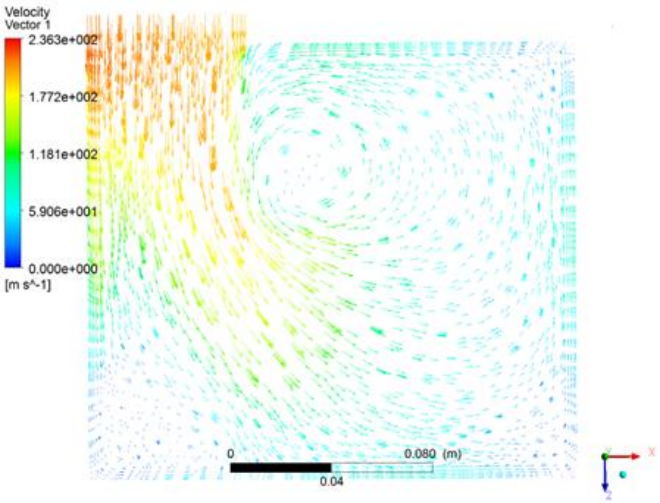

(a)

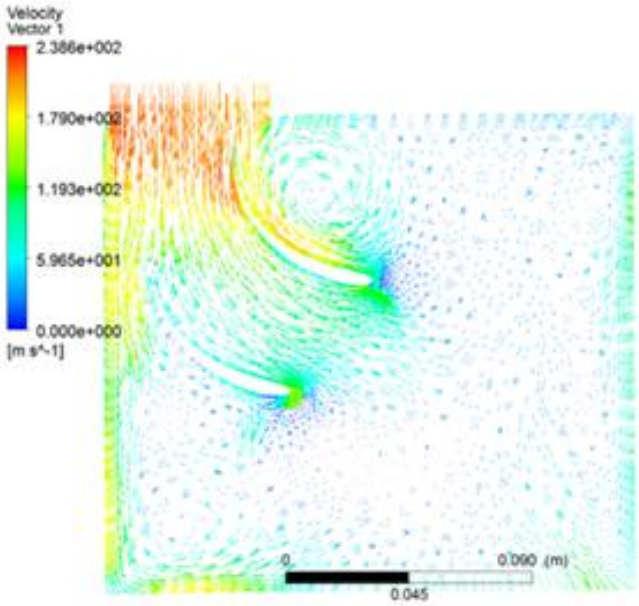

(b)

Figure 4.12: Velocity magnitude (m^2/s) vector plot: (a) lower part air box without guide vane; (b) lower part air box with guide vane

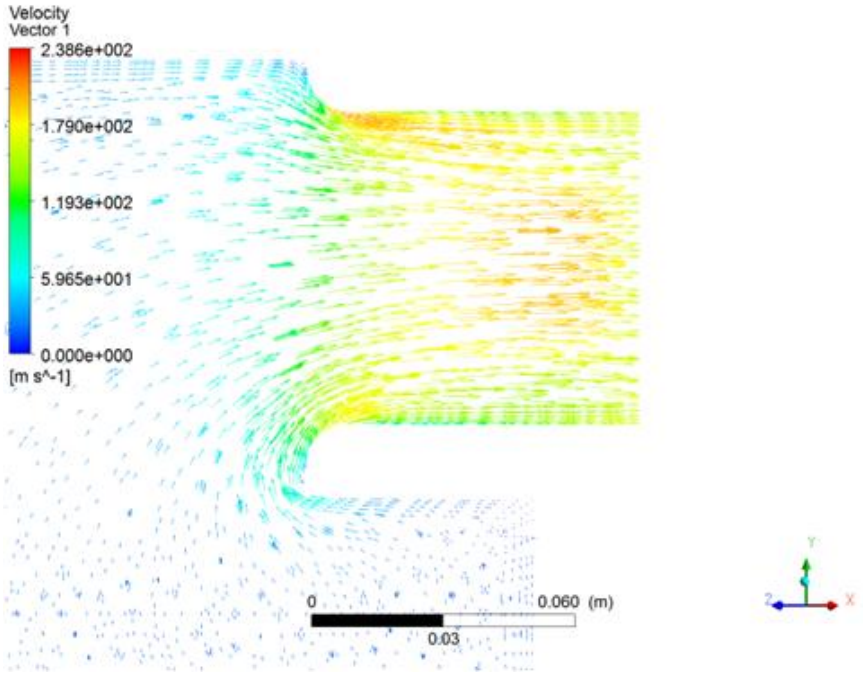

(a)

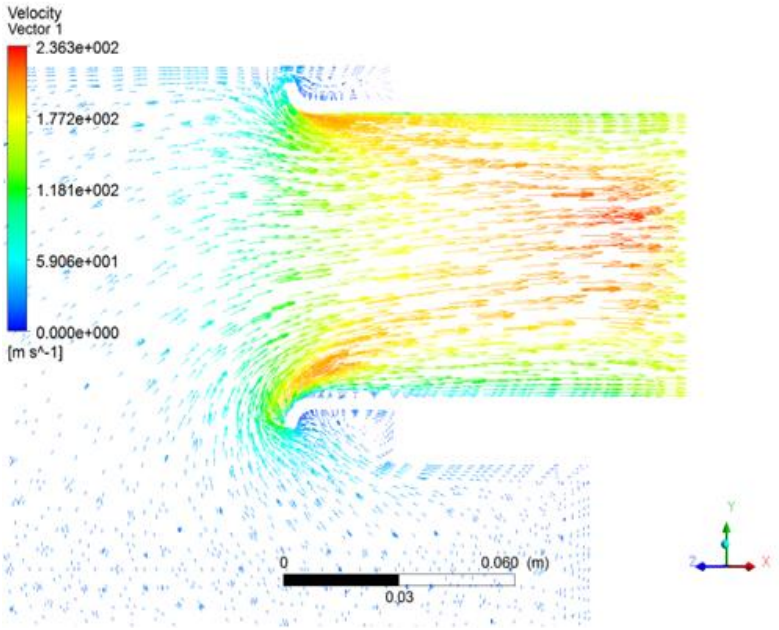

(b)

Figure 4.13: Velocity magnitude (m^2/s) vector plot: (a) upper part air box without bell mouth; (b) upper part air box with bell mouth

4.3.2 Experimental results

The results of flow bench test at test pressure 25 cmH_2O for standard and optimized air box have been obtained and will be analyzed in this section.

Table 4.6: Result of pressure drop for flow bench test on standard air box at valve lift 0.001 m until 0.008 m

Valve Lift (m)	Flow Rate (L/s)	h_1, inlet (m)	h_2, outlet (m)	P_1, inlet (Pa)	P_2, outlet (Pa)	P_1-P_2, Pressure Drop (Pa)
0.001	3	0.000	0.001	101325.00	101315.19	9.81
0.002	8	0.001	0.004	101315.19	101285.76	29.43
0.003	15	0.003	0.011	101295.57	101217.09	78.48
0.004	21	0.004	0.016	101285.76	101168.04	117.72
0.005	27	0.007	0.023	101256.33	101099.37	156.96
0.006	32	0.009	0.030	101236.71	101030.70	206.01
0.007	34	0.010	0.034	101226.90	100991.46	235.44
0.008	36	0.011	0.037	101217.09	100962.03	255.06

Table 4.7: Result of pressure drop for flow bench test on optimized air box with guide vane and bell mouth at valve lift 0.001 m until 0.008 m

Valve Lift (m)	Flow Rate (L/s)	h_1, inlet (m)	h_2, outlet (m)	P_1, inlet (Pa)	P_2, outlet (Pa)	P_1-P_2, Pressure Drop (Pa)
0.001	3	0.000	0.001	101325.00	101315.19	9.81
0.002	8	0.001	0.003	101315.18	101295.57	19.61
0.003	15	0.003	0.010	101295.54	101226.90	68.64
0.004	21	0.004	0.015	101285.72	101177.85	107.87
0.005	27	0.005	0.019	101275.91	101138.61	137.29
0.006	32	0.007	0.026	101256.27	101069.94	186.33
0.007	34	0.009	0.031	101236.63	101020.89	215.74
0.008	36	0.012	0.036	101207.17	100971.84	235.33

Table 4.8: Result of pressure drop for flow bench test on optimized air box with guide vane at valve lift 0.001 m until 0.008 m

Valve Lift (m)	Flow Rate (L/s)	h_1, inlet (m)	h_2, outlet (m)	P_1, inlet (Pa)	P_2, outlet (Pa)	P_1-P_2, Pressure Drop (Pa)
0.001	3	0.000	0.001	101325.00	101315.19	9.81
0.002	8	0.001	0.004	101315.19	101285.76	29.43
0.003	15	0.001	0.009	101315.19	101236.71	78.48
0.004	21	0.003	0.016	101295.57	101168.04	127.53
0.005	27	0.006	0.023	101266.14	101099.37	166.77
0.006	32	0.008	0.030	101246.52	101030.70	215.82
0.007	34	0.011	0.036	101217.09	100971.84	245.25
0.008	36	0.013	0.041	101197.47	100922.79	274.68

Table 4.9: Result of pressure drop for flow bench test on optimized air box with bell mouth at valve lift 0.001 m until 0.008 m

Valve Lift (m)	Flow Rate (L/s)	h_1, inlet (m)	h_2, outlet (m)	P_1, inlet (Pa)	P_2, outlet (Pa)	P_1-P_2, Pressure Drop (Pa)
0.001	3	0.000	0.001	101325.00	101315.19	9.81
0.002	8	0.001	0.003	101315.19	101295.57	19.62
0.003	15	0.002	0.009	101305.38	101236.71	68.67
0.004	21	0.005	0.016	101275.95	101168.04	107.91
0.005	27	0.008	0.021	101246.52	101118.99	127.53
0.006	32	0.010	0.028	101226.90	101050.32	176.58
0.007	34	0.014	0.035	101187.66	100981.65	206.01
0.008	36	0.015	0.038	101177.85	100952.22	225.63

The curve for pressure drop with point was plotted to see the difference between the pressure drop at each valve lift for standard air box part, optimized air box part with guide vane, optimized air box part with bell mouth, and optimized air box part with guide vane and bell mouth respectively. Figure 4.13, 4.14, 4.15, 4.16, 4.17, and Figure 4.18 show the comparison of pressure drop between the air box parts from valve lift 0.001 m until valve lift 0.008 m.

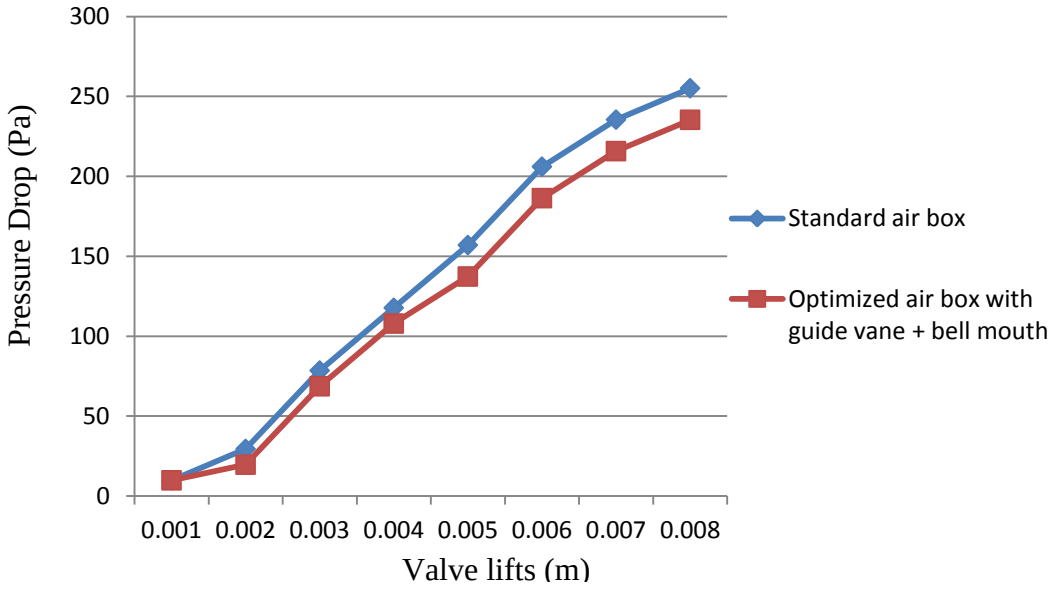

Figure 4.14: Graph of pressure drop versus valve lift for flow bench test on standard air box and optimized air box with guide vane and bell mouth at 0.001 m valve lift until 0.008 m valve lift.

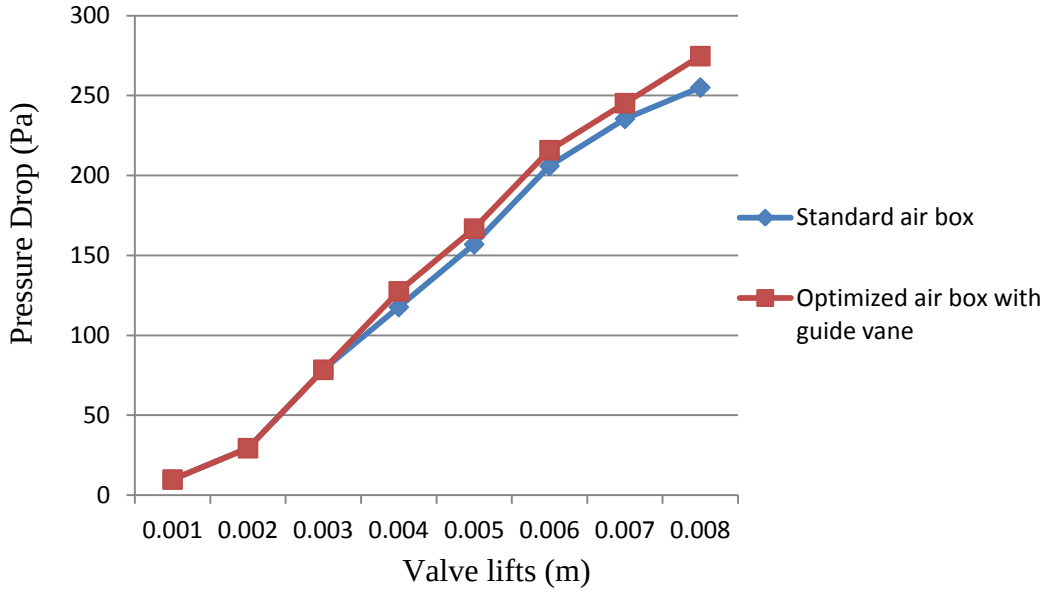

Figure 4.15: Graph of pressure drop versus valve lift for flow bench test on standard air box and optimized air box with guide vane at 0.001m valve lift until 0.008m valve lift.

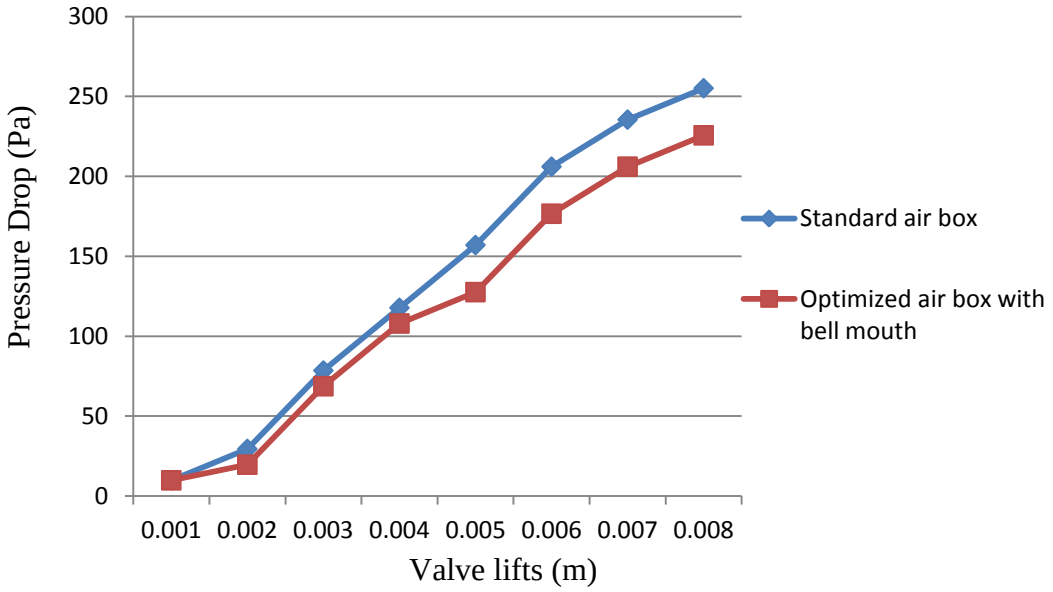

Figure 4.16: Graph of pressure drop versus valve lift for flow bench test on standard air box and optimized air box with bell mouth at 0.001 m valve lift until 0.008 m valve lift.

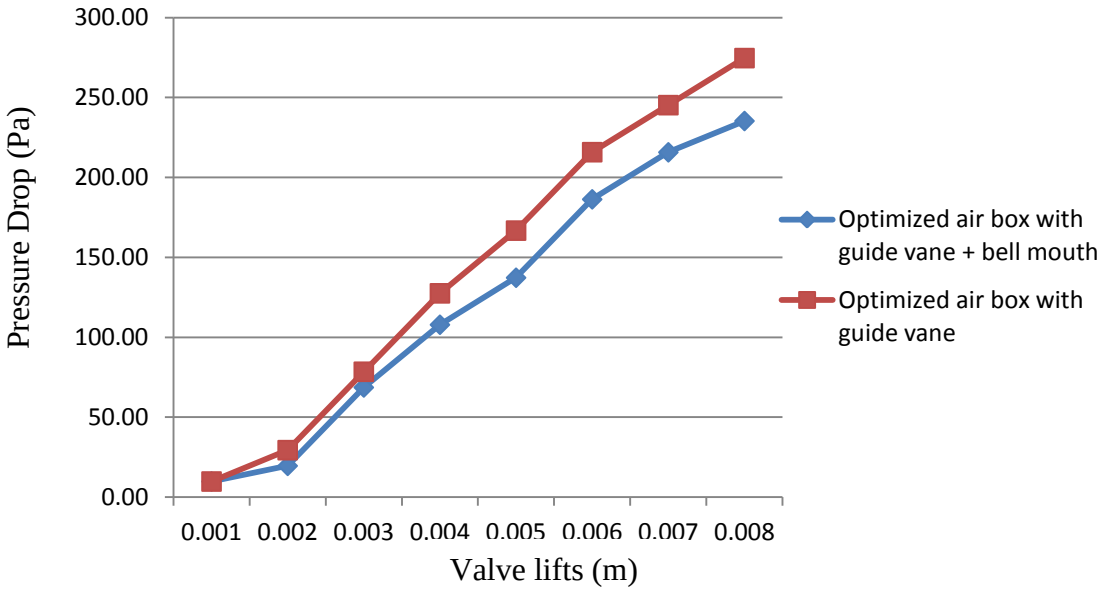

Figure 4.17: Graph of pressure drop versus valve lift for flow bench test on optimized air box with guide vane and bell mouth and optimized air box with guide vane at 0.001 m valve lift until 0.008 m valve lift.

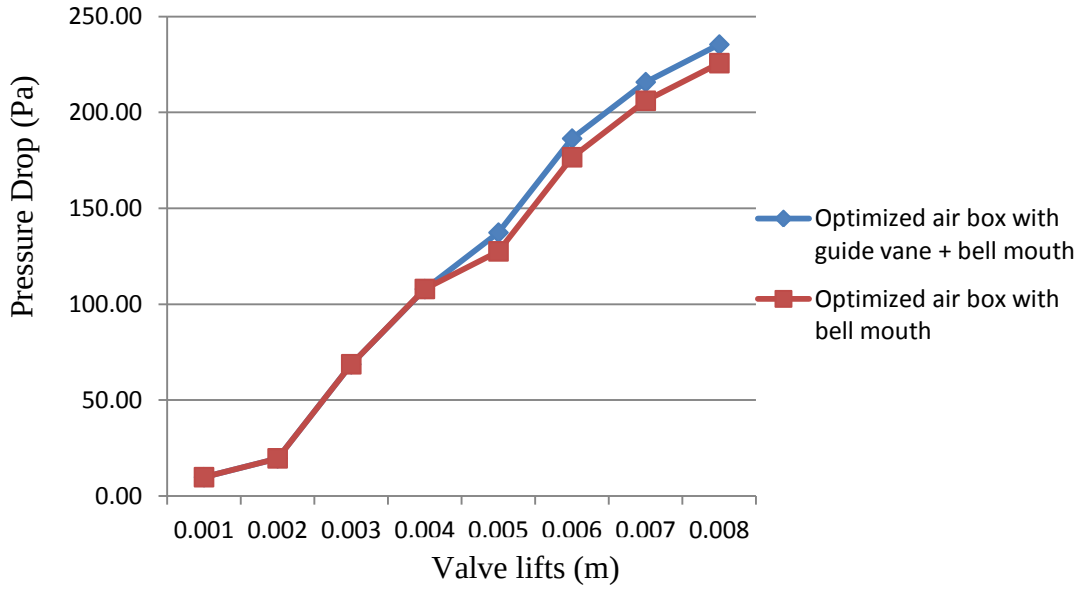

Figure 4.18: Graph of pressure drop versus valve lift for flow bench test on optimized air box with guide vane and bell mouth and optimized air box with bell mouth at 0.001 m valve lift until 0.008 m valve lift.

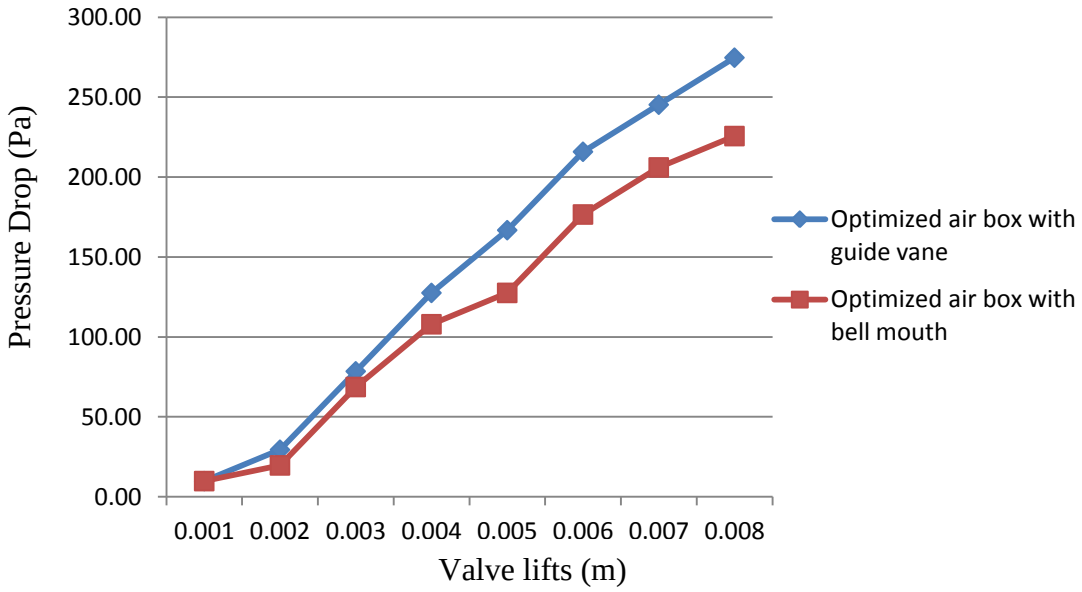

Figure 4.19: Graph of pressure drop versus valve lift for flow bench test on optimized air box with guide vane and optimized air box with bell mouth at 0.001 m valve lift until 0.008 m valve lift.

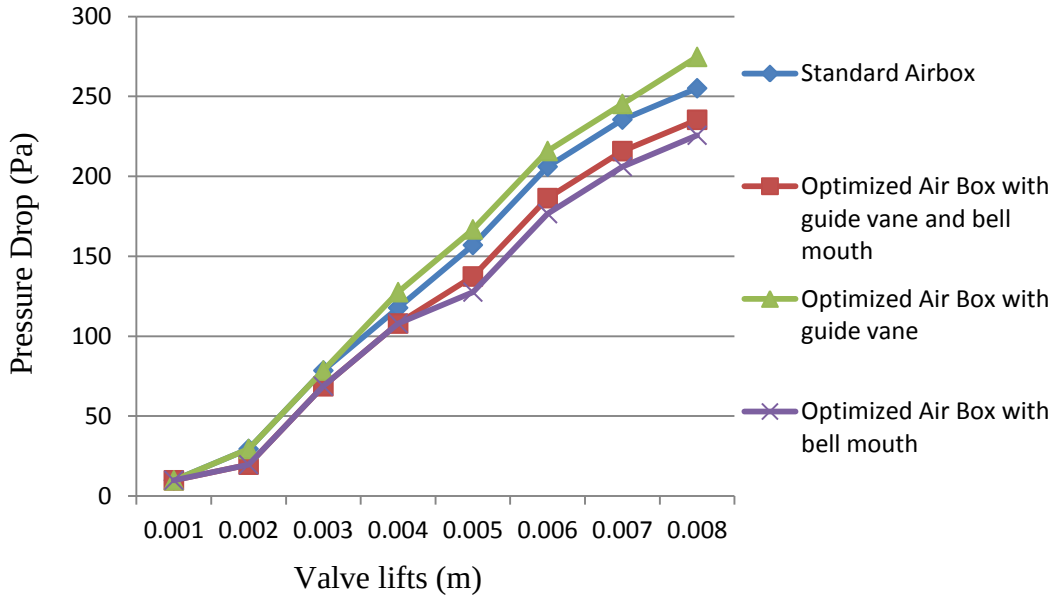

Figure 4.20: Graph of pressure drop versus valve lift for flow bench test on standard air box, optimized air box with guide vane and bell mouth, optimized air box with guide vane and optimized air box with bell mouth at 0.001 m valve lift until 0.008 m valve lift.

At valve lift 0.008 m, optimized air box with guide vane has the highest value of pressure drop, which is 274.68 Pa. For the lowest value of pressure drop at valve lift 0.008 m, optimized air box with bell mouth gives the lowest value which is 225.63 Pa.

(Calculation of pressure drop for optimized air box with guide vane at valve lift 0.008m)

P_{atm} $= P_{H2O} + P_{inlet}$

P_{inlet} $= P_{atm} - P_{H2O}$

$= 101325 - P_{inlet}$

Pressure drop, ΔP $= P_{inlet} - P_{outlet}$

$$P_{H2O} = \rho_{water} g h_1$$

Where,

ρ_{water} = 1000 (kg/m³)

g = 9.81 (m/s²)

h_1 = inlet water height (m), from manometer

P_{inlet} = 101325 – (1000)(9.81)(0.013)

= 101197.47 Pa

P_{outlet} = 101325 – (1000)(9.81)(0.041)

= 100922.79 Pa

Pressure drop, ΔP = $P_{inlet} - P_{outlet}$

= 101197.47 - 100922.79

= 274.68 Pa

4.4 DISCUSSIONS

The results obtain from the study will be discussed in this section. The results are divided into two types of analysis, which are CFD analysis and flow bench test analysis.

4.4.1 CFD analysis

From CFD analysis, at higher RPM rate, the pressure drop will increase due to air restriction inside the air box. The variations of RPM with the pressure drop for different air box are shown in Table 4.2 until Table 4.5. Different design of an air box will give a different pattern of pressure drop because each design of air box has different restriction area inside the air box.

In CFD simulation condition setup, an optimized air box with bell mouth gives the lowest value of pressure drop since the installation of bell mouth can avoid separation and recirculation of flow at the outlet. Thus it can reduce the pressure drop inside the air box. For guide vane installation, the pressure drop inside the air box will increase since the restriction area occurred at guide vane because there is no ram air velocity considered at the inlet in this simulation. Despite the pressure drop was increased, the guide vane allows air from the inlet to be distributed uniformly inside the lower part of air box and being filtered efficiently. Thus optimize the air filtering process.

CFD analysis on the combination of guide vane and bell mouth installation on an air box shows that the pressure drop was still lower than the standard air box. Thus optimized air box with guide vane and bell mouth design was good since it reduced the pressure drop and increases the air filtering efficiency.

4.4.2 Flow bench test analysis

In flow bench test analysis, outlet velocity cannot be set in some fixed value. Therefore, valve lift open was set in an increment of 0.001 from 0.001 m valve open to control the air flow rate through the air box. The value of water height of the manometer at inlet (h_1) and outlet (h_2) were recorded and tabulated to measure the pressure at inlet and outlet of the air box.

After the flow bench test was done, the experimental data have been compared with the CFD simulation results. The experimental data value might be different from the simulation result due to the different control parameter. However, the pressure drop comparison between the different air box designs on the flow bench test shows the same result as the simulation test. The optimized air box with bell mouth gives the lowest value of pressure drop among others design at valve open 0.008 m which is 225.63 Pa.

Some errors may occur during the flow bench test such as leaking on head adapter, fluctuate air temperature, and error on the dial gauge. These may result on a different percentage of pressure drop between CFD results and experiment results.

CHAPTER 5

CONCLUSION AND RECOMMENDATION

5.1 CONCLUSION

Generally, 3-D model of an air box has been developed while conducting this study. The pressure drops inside air box designs also have been tabulated from this study. CFD analysis and flow bench test on standard air box, optimized air box with guide vane and bell mouth, optimized air box with guide vane, and optimized air box with bell mouth have been conducted. In CFD simulation test, optimized air box with bell mouth gives the lowest pressure drop at 7000 RPM compared to the other air box design which was 22098.188 Pa. Followed by optimized air box with guide vane and bell mouth which was 22923.01 Pa, standard air box, which was 23847.11 Pa, and optimized air box with guide vane, which was 28807.80 Pa. In flow bench testing analysis, optimized air box with bell mouth also gives the lowest pressure drop among others design, which was 225.63 Pa at valve open 0.008 m. Followed by optimized air box with guide vane and bell mouth which was 235.33Pa, standard air box which was 255.06 Pa, and optimized air box with guide vane which was 274.68 Pa. From the results obtain, optimized design of an air box has been developed.

5.2 RECOMMENDATION

In this present studied, a lot of problems were faced when doing the experiments. For continuing this project or further research, some of the recommendations were made and should be considered for better analysis and accuracy results. Performance of flow bench machine should be checking first before do the experiment such as make sure there was no air leaking at the head adapter or at air intake system while doing test. Air leaking will affect the result's accuracy in flow bench test. For better accuracy on getting pressure drop, use micro manometer since it will give better reading. The test section at the inlet and outlet of the air box must have a good condition in order to get good pressure measurement. For the future study, having good instrument devices was a must for taking best and effectively data have.

REFERENCES

Ceviz M.A., M.A., *Design of a new SI engine intake manifold with variable length plenum.* Energy Conversion and Management, 2010. 51(11): p. 2239-2244.

Makgata, K.W., *Computational Analysis And Optimisation of The Inlet System Of A High-Performance Rally Engine*, in *Mechanical Engineering*. 2005, University of Pretoria. p. 122.

Holger Paffrath, M.A., Karl-Ernst Hummel, *Technology for Future Air Intake Systems.* SAE Technical Paper, 1999. 1999-01-0266.

Ceviz, M.A., *Intake plenum volume and its influence on the engine performance, cyclic variability and emissions.* Elsevier, 2007. 48(961–966).

Rizalman Mamat, A.-F.M.M., Hongming Xu and Miroslaw L. Wyszynski, *CFD Analysis of Air Intake System with Negative Pressure on Intake Grill.* SAE Technical Paper, 2008. 2008-01-1643.

John A. Vfhiie Jr., J.C.W., *Air Cleaner Shell Noise Reduction with Finite Element Shape Optimization.* SAE Technical Paper, 1997. 971876.

B. Murali Krishna, A.B., and J. M. Mallikarjuna, *Effect of Intake Manifold Inclination on Intake Valve Flow Characteristics of a Single Cylinder Engine using Particle Image Velocimetry.* World Academy of Science, Engineering and Technology, 2010. 68.

D. Ramasamy, Z.M., S.Mahendran, S. Vijayan, *Design Optimization of Air Intake System (AIS) of 1.6L Engine by Adding Guide Vane.* IMECS, 2010. 2.

Hyunsoo Jung., K.-J.C., *Development of Air Intake System for Sporty Coupe Using the Robust Design Method.* SAE Technical Paper, 2009.

Wolfgang Foken, S.P., West Saxon, *Test Bench for the Acoustic Behaviour of Air-Boxes for Motorcycles.* SAE Technical Paper, 2002. 2002-32-1812.

Ravinder Yerram, N.P., Prakash Rao Malathkar, Vasudeo Halbe, Shashidhara Murthy K., *Optimization of Intake System and Filter of an Automobile using CFD analysis.* QuEST, 2006.

A. Aroussi, S.A.A.G., B. S. AbdulNour, *Demisting of Vehicle Air Intake Using Plane Baffles.* SAE Technical Paper, 2003. 2003-01-1077.

A. S. Patil and V. G. Halbe, K.C.V., *A System Approach to Automotive Air Intake System Development.* SAE Technical Paper, 2005. 2005-26-011.

Safari, M., Nasiritosi, A., Ghamari, M. , *Intake Manifold Optimization by using 3D- CFD Analysis.* SAE Technical Paper, 2003. 2003-32-0073.

Rizalman Mamat, N.R.A., Hongming Xu, Miroslaw L. Wyszynski, Athanasios Tsolakis, *Effect of Air Intake Pressure Drop on Performance and Emissions of a Diesel Engine Operating with Biodiesel and Ultra Low Sulphur Diesel (ULSD).* ICREPQ, 2009.

Morton, D.W., *Match the Engine Intake System to the Application and Environment.* SAE Technical Paper, 1970. 700533.

Karthikeyan S. , R.H., M. Sathyanadan, S. Krishnan, P. Vadivel, D.Vamsidhar, *Computational Analysis Of Intake Manifold Design And Experimental Investigation On Diesel Engine For LCV*. IJEST, 2011. 3(2359).

Ravindra Devi, P.S., Brian Walter, Barry Record, Veera Rajendran, *Pressure Reduction in Intake System of a Turbocharged-Inter Cooled DI Diesel Engine Using CFD Methodology*. SAE Technical Paper, 2004. 2004-01-1874.

Heywood, J.B (1988), *Internal Combustion Engine Fundamental*, McGraw Hill, New York

Kriel, J.B., *Engine Performance Improvement by Modeling of Airflow Through Intake Manifold*, in *Mechanical Engineering*. 2008, Tshwane University of Technology. p. 212.

Nak W. Sung, J.S.C., Young I. Jeong, *A Study on the Flow in the Engine Intake System.* SAE Technical Paper, 1995. 952067.

John D. F., Gasiorek, J.M., Swaffield, J.A.,, *Fluid Mechanics*, ed. L.G.U. Kingdom. 2005: Pearson.

Hirsch, *Numerical computation of internal and external flows: fundamentals of computational fluid dynamics*. 2 ed. 2007: John Wiley & Sons

Lim, S.C., Haecheon, *Optimal Shape Design of a Two-Dimensional Asymmetric Diffuser in Turbulent Flow.* AIAA, 2004. 42(6): p. 1154-1169

Alex., M., *Air Intake Development - Effects of Coupled Fluid/Structure Modes.* SAE Technical Paper, 2001. 2001-01-1431.

Negin Maftouni, R.E., *Intake Manifold Optimization by Using 3-D CFD Analysis With Observing The Effect of Length of Runners On Volumetric Efficiency*. ASME, 2006.

Francesco Gamba, L.P., Giovanni Turino, *Optimized Air Intake Systems.* SAE Technical Paper, 1995. 951264.

John J. Silvestri, T.M., Michael Costello, *Study of Intake System Wave Dynamics and Acoustics by Simulation and Experiment.* SAE Technical Paper, 1994. 940206.

V Ganesan, J.S.K., V.Balasubramanian, *Flow Field Analysis of A Multi Cylinder S.I. Engine Air Intake System Using Computational Fluid Dynamics.* 2004. 2004-28-0010.

White, FM (1991), *Viscous Fluid Flow*, Second Edition, McGraw-Hill International, New York.

White, FM (1994), *Fluid Mechanics*, Third Edition, McGraw-Hill International, New York

Talha I Khan., M.J., *Modelling and Flow Behaviour Analysis of Inner Plenum using Computational Fluid Dynamics (CFD).* European Journal of Scientific Research, 2011. 56(3): p. 346-353.

Tennekes H., J.L.L., *A First Course In Turbulence*. 1994, United States of America: Kingsport Press.

Mohamed Ali Jemni, G.K., Mohamed Salah Abid, *Influence of intake manifold design on in-cylinder flow and engine performances in a bus diesel engine converted to LPG gas fuelled, using CFD analyses and experimental investigations.* Elsevier, 2011. 36.

Arcoumanis C, Kamimoto T. *Flow and combustion in reciprocating engines*. Berlin Heidelberg: Springer-Verlag; 2009.

Poroseva SV, Bezard H. *On ability of standard k-3 model to simulate aerodynamic turbulent flows*. CFD J; 2001:627e33. Special Number 2001.

Fergizer, JH, *Computational Methods for Fluid Dynamics*, Third Ed., Springer, 2002, Berlin.

Vinodh Kumar B., S.N., Gopalakrishnan N., *Air Flow and Charge Motion Study of Engine Intake Port.* 2010.

Ismail A. R., R.A.Bakar., Semin, *An Investigation of Valve Lift Effect on Air Flow and CD of Four Stroke Engines Based on Experiment.* American Journal of Applied Sciences, 2008. 5(8): p. 963-971.

S. A. Sulaiman, S.H.M.M., I. Ibrahim and Z. A. Abdul Karim, *Study of Flow In Air-Intake System For A Single-Cylinder Go-Kart Engine.* IJAME, 2010. 1: p. 91-104.

Athanasios G. Konstandopoulos, E.S., James Warren, Ronny Allansson, *Optimized Filter Design and Selection Criteria for Continuously Regenerating Diesel Particulate Traps.* SAE Technical Paper, 1999. 1999-01-0468.

APPENDICES A

GANTT CHART FOR FINAL YEAR PROJECT (FYP) 1

Project Activities	W1	W2	W3	W4	W5	W6	W7	W8	W9	W10	W11	W12	W13	W14
Meeting and briefing FYP with SV														
Find information about project title														
Complete Chapter 1														
Find literature review														
Construct Chapter 2														
Find information about methodology														
Discuss with SV about experiment														
Complete Chapter 3														
Design model using SolidWork														
Submit Chapter 1,2,3														
Prepare for FYP 1 presentation														

APPENDICES B

GANTT CHART FOR FINAL YEAR PROJECT (FYP) 2

Project Activities	W1	W2	W3	W4	W5	W6	W7	W8	W9	W10	W11	W12	W13	W14
Model analysis using ANSYS 12.1														
Simulation in Fluent														
Model fabrication														
Flowbench Test														
Compare both result														
Complete Chapter 4														
Submit chapter 4														
Make conclusion														
Report finalize														
Preparing for final presentation														